

LoCuSS: Connecting the Dominance and Shape of Brightest Cluster Galaxies with the Assembly History of Massive Clusters

Graham P. Smith,^{1,2*} Habib G. Khosroshahi,^{3,4†} A. Dariush,^{1,5} A. J. R. Sanderson,¹
T. J. Ponman,¹ J. P. Stott,³ C. P. Haines,¹ E. Egami,⁶ D. P. Stark⁷

¹ School of Physics and Astronomy, University of Birmingham, Edgbaston, Birmingham, B15 2TT, England

² California Institute of Technology, Mail Code 105–24, Pasadena, CA 91125, USA

³ School of Astronomy, Institute for Studies in Theoretical Physics and Mathematics (IPM), Tehran, Iran

⁴ Astrophysics Research Institute, Liverpool JMU, Twelve Quays House, Egerton Wharf, Birkenhead, CH41 1LD, England

⁵ Cardiff School of Physics and Astronomy, Cardiff University, Queens Buildings, The Parade, Cardiff, CF24 3AA, Wales

⁶ Steward Observatory, University of Arizona, 933 North Cherry Avenue, Tucson, AZ 85721, USA

⁷ Institute of Astronomy, University of Cambridge, Madingley Road, Cambridge, CB3 0HA, England

*Email: gps@star.sr.bham.ac.uk

†Email: habib@ipm.ir

Accepted, Received

ABSTRACT

We study the luminosity gap, Δm_{12} , between the first and second ranked galaxies in a sample of 59 massive ($\sim 10^{15} M_{\odot}$) galaxy clusters, using data from the Hale Telescope, the *Hubble Space Telescope* (*HST*), *Chandra*, and *Spitzer*. We find that Δm_{12} distribution, $p(\Delta m_{12})$, is a declining function of Δm_{12} , to which we fitted a straight line: $p(\Delta m_{12}) \propto -(0.13 \pm 0.02)\Delta m_{12}$. The fraction of clusters with “large” luminosity gaps is $p(\Delta m_{12} \geq 1) = 0.37 \pm 0.08$, which represents a 3σ excess over that obtained from Monte Carlo simulations of a Schechter function that matches the mean cluster galaxy luminosity function. We also identify four clusters with “extreme” luminosity gaps, $\Delta m_{12} \geq 2$, giving a fraction of $p(\Delta m_{12} \geq 2) = 0.07_{-0.03}^{+0.05}$. More generally, large luminosity gap clusters are relatively homogeneous, with elliptical/disky brightest cluster galaxies (BCGs), cuspy gas density profiles (i.e. strong cool cores), high concentrations, and low substructure fractions. In contrast, small luminosity gap clusters are heterogeneous, spanning the full range of boxy/elliptical/disky BCG morphologies, the full range of cool core strengths and dark matter concentrations, and have large substructure fractions. Taken together, these results imply that the amplitude of the luminosity gap is a function of both the formation epoch, and the recent infall history of the cluster. “BCG dominance” is therefore a phase that a cluster may evolve through, and is not an evolutionary “cul-de-sac”. We also compare our results with semi-analytic model predictions based on the Millennium Simulation. None of the models are able to reproduce all of the observational results on Δm_{12} , underlining the inability of the current generation of models to match the empirical properties of BCGs. We identify the strength of AGN feedback and the efficiency with which cluster galaxies are replenished after they merge with the BCG in each model as possible causes of these discrepancies.

Key words: galaxies:clusters:general – galaxies:elliptical – galaxies:halos – X-ray:galaxies – X-rays:galaxies:clusters – gravitational lensing

1 INTRODUCTION

Numerical simulations and large-scale redshift surveys both indicate that we live in a hierarchical universe, i.e. one in which the large-scale structure of the universe grows from the bottom up with smaller objects forming earlier than larger objects. This picture rests on the matter content of the universe being dominated by collisionless dark matter particles, smoothly distributed at early times, and seeded with small density perturbations. Exploring this picture

observationally in the non-linear regime of gravitational collapse, i.e. within collapsed dark matter halos that host individual galaxies through to massive clusters of galaxies, complements the statistical analysis of the linear regime probed by galaxy redshift surveys. Indeed, a promising route to fleshing out our understanding of hierarchical structure formation is to measure observable quantities that are sensitive to the age and/or assembly history of dark matter halos, and thus in principle to test the hierarchical paradigm by comparing the observed and predicted distributions. Any dis-

crepancies found between observation and theory may ultimately point to modifications to the theoretical model including, for example, the properties of the dark matter particle and the distribution of initial density fluctuations (e.g. Komatsu et al. 2009). Quantities discussed in the literature that may be useful probes of the age and assembly history of dark matter halos include the luminosity gap between the first and second ranked galaxies in a group or cluster (often expressed as the difference between their magnitudes, $\Delta m_{12} = m_1 - m_2$; e.g. Dariush et al. 2007), the concentration of dark matter halos (e.g. Neto et al. 2007; Okabe et al. 2010), and the sub-halo population of dark matter halos (e.g. Taylor & Babul 2004; Zentner et al. 2005).

The luminosities of the first and second ranked galaxies in clusters was first studied, as far as we are aware, by Sandage & Hardy (1973, see also Geller et al. 1976; Tremaine et al. 1977; Ostriker & Hausman 1977; Oegerle & Hoessel 1989). More recently the luminosity gap, Δm_{12} , was studied in the context of galaxy groups, the term “fossil” being coined to describe virialized systems with $\Delta m_{12} \geq 2$ (Ponman et al. 1994; Jones et al. 2000, 2003). L^* galaxies are absent from fossil groups, which were thus interpreted as having formed at early times, with dynamical friction then having sufficient time to cause the L^* galaxy population to merge and form the brightest group galaxy (BGG). Fossil groups are expected to be more common than fossil clusters, at least in part because the probability of galaxy-galaxy merging is anti-correlated with galaxy velocity, and thus with cluster mass. Nevertheless, two clusters with masses of $\sim 10^{14} M_\odot$ have been found with $\Delta m_{12} > 2$ (Khosroshahi et al. 2006; Mendes de Oliveira et al. 2006; Cypriano et al. 2006). These two objects (RXJ1416.4+2315, and RXJ15552.2+2013) raise the interesting question of whether the most massive ($\gtrsim 10^{15} M_\odot$) clusters might host similarly dominant BCGs. Theoretical studies suggest that this is the case, for example, Milosavljević et al. (2006) and Dariush et al. (2007) predict that $\sim 1 - 3\%$ and $\sim 5\%$ of $10^{15} M_\odot$ clusters have $\Delta m_{12} \geq 2$ respectively.

The concentration parameter of a dark matter halo describes the shape of its density profile following the so-called universal profile proposed by Navarro et al. (1997) and variants thereon. Halos with smaller concentrations have a flatter density profile, while larger concentrations imply a steeper density profile. Bullock et al. (2001) analyzed numerical simulations of CDM universes finding a weak dependence of concentration on halo mass: $c \propto M^\alpha$ with $\alpha \simeq -0.1$ (see also Dolag et al. 2004; Neto et al. 2007; Duffy et al. 2008). This relationship arises from the relative timing of the formation of dark matter halos as a function of mass. On average less massive halos form at earlier times than more massive halos in a hierarchical universe. At earlier times the universe was denser than at later times, and thus the central regions of less massive halos are relatively dense, leading to higher concentration parameters than for more massive halos. Some observational studies have reported very high concentration parameters in individual systems, for example, one of the fossil groups studied by Khosroshahi et al. (2004, 2006) was found to have $c > 50$, based on modeling of X-ray observations. Lensing studies of several individual strong-lensing clusters have also obtained very high concentrations of $c \sim 10$ in contrast to the theoretical prediction of $c \sim 5$ (Kneib et al. 2003; Gavazzi 2003; Broadhurst et al. 2005; Limousin et al. 2007). More recently, observational studies have begun to study larger samples and thus to constrain the concentration-mass relation itself, and to probe the general population rather than a small number of potentially extreme objects (e.g. Buote et al. 2007; Okabe et al. 2010).

Theoretically, substructures within dark matter halos, i.e. the sub-halo population, are also sensitive to the assembly history of the host dark matter halo (e.g. Taylor & Babul 2004; Zentner et al. 2005). Observationally substructures in galaxy clusters can be identified via detailed modeling of the observed gravitational lensing signal (Smith et al. 2005, 2009; Richard et al. 2010a,b). Specifically, group- and galaxy-scale perturbers are required to achieve statistically acceptable fits to the strong-lensing data. The contribution of these structures to the total cluster mass is quantified via the “substructure fraction”, f_{sub} , defined as the amount of mass within the adopted cluster-centric radius that is assigned to substructures divided by the total cluster mass within the same aperture. Smith & Taylor (2008) combined Smith et al.’s (2005) observational measurements of f_{sub} for 10 X-ray luminous galaxy clusters with Taylor & Babul’s (2004) semi-analytic model of structure formation to explore the interpretation of lensing-based measurements of f_{sub} . The main conclusion was that f_{sub} depends on both when the cluster formed, and on the level of recent mass assembly, each defined as the lookback time to when each cluster had acquired 50% and 90% of their observed mass respectively. For example: clusters at $z = 0.2$ with $f_{\text{sub}} < 0.1$ formed on average at $z \gtrsim 0.8$, and suffered $\leq 10\%$ mass growth since $z = 0.4$; in contrast, clusters at $z = 0.2$ with the highest substructure fractions ($f_{\text{sub}} \gtrsim 0.4$) formed on average since $z \simeq 0.4$ and acquired $\gtrsim 10\%$ of their mass between $z = 0.25$ and $z = 0.2$, i.e. a time interval of just 500Myr.

A complementary view of hierarchical merging within galaxy clusters is available from BCG morphology. Based on their isophotal shapes, elliptical galaxies have been classified as disky or boxy (Bender et al. 1989) – with positive and negative fourth-order Fourier coefficients respectively. The interpretation of boxy and disky isophotes in terms of the details of galaxy merger histories is a controversial subject (Faber et al. 1997; Naab & Burkert 2003; Khochfar & Burkert 2005). In this study we will side-step these difficulties, and concentrate simply on disky/boxy isophotes as an indicator of the presence of gas that has dissipated, and settled into a disk-like structure, either because the last massive galaxy to merge with the BCG was gas rich, or because gas has been accreted by the merger product from its environment, e.g. by a BCG in a cool core cluster. BCGs are the most massive early-type galaxies and are generally expected to have boxy isophotes consistent with formation via mergers of early-type (gas-poor) galaxies (Lin & Mohr 2004; Khosroshahi, Ponman & Jones 2006). However, BGGs in some fossil groups are as bright as BCGs and do *not* have boxy isophotes (Khosroshahi, Ponman & Jones 2006), suggesting that (i) fossil BGGs may form early from the mergers between gas-rich spiral galaxies, and (ii) some fossil BGGs may have subsequently evolved into BCGs.

The main aim of this article is to combine measurements of the luminosity gap, cool core strength, concentration, substructure fraction, and BCG isophotal shape for a large sample of clusters to assemble an empirical picture of the hierarchical assembly of clusters and their BCGs. We present the first observational measurement of the distribution of the luminosity gap statistic of $10^{15} M_\odot$ clusters, and compare this distribution with the other probes of hierarchical assembly discussed above. This allows us to build an empirical picture with which to assess the usefulness of the respective measurements for assessing the age of clusters. We also investigate how well the current generations of galaxy formation models can reproduce the observed luminosity gap distribution. The data used for this study are drawn from the Local Cluster Substructure Survey (LoCuSS; PI: Smith; <http://www.sr.bham.ac.uk/locuss>). A

summary of LoCuSS is provided in §2, together with a description of the data used in this paper. The analysis and results are then presented in §3, and compared with theoretical predictions in §4. The main conclusions are summarized and discussed in §5. We assume $H_0=70 \text{ km s}^{-1} \text{ Mpc}^{-1}$, $\Omega_M=0.3$ and $\Omega_\Lambda=0.7$ throughout. In this cosmology $1''$ corresponds to a physical scale of 3.3kpc, at $z=0.2$. All photometric measurements are relative to Vega.

2 DATA

2.1 Sample Selection and Observing Strategy

LoCuSS is a morphologically-unbiased multi-wavelength survey of X-ray luminous galaxy clusters at $0.15 \leq z \leq 0.3$. The overall aim of the survey is to measure the cluster-cluster scatter in key observables such as the X-ray temperature, and Y_X parameter (Smith et al. 2005; Zhang et al. 2008; Okabe et al. 2010), the Sunyaev-Zeldovich Effect Y parameter (Marrone et al. 2009), and the obscured and unobscured star formation activity (Haines et al. 2009a,b, 2010; Smith et al. 2010; Pereira et al. 2010), and to correlate this scatter with the structure and thus hierarchical assembly history of the clusters. The backbone of the survey is the gravitational lensing analysis of *HST* (Smith et al. 2005; Richard et al. 2010b, Hamilton-Morris et al. in prep.; May et al. in prep.) and Subaru (Okabe et al. 2010; Oguri et al. 2010) imaging data, because the lensing-based mass maps can be used to infer the likely assembly history of the clusters (Smith & Taylor 2008).

The parent sample for this study comprises 115 clusters satisfying $-27^\circ \leq \delta \leq 70^\circ$, $0.15 \leq z \leq 0.3$, $n_H \leq 7 \times 10^{20} \text{ cm}^{-2}$ drawn from the ROSAT All-sky Survey catalogs (Ebeling et al. 1998, 2000; Böhringer et al. 2004). The cut at $\delta = -27^\circ$ ensures that the clusters are observable from Palomar Observatory at elevations above 30° (an airmass of $\sec z \leq 2$). The clusters span a decade in X-ray luminosity in the $0.1 - 2.4 \text{ keV}$ band: $2 \times 10^{44} \lesssim L_X \lesssim 20 \times 10^{44} \text{ erg s}^{-1}$ (Fig. 1), which corresponds to a mass range of $5 \times 10^{14} \lesssim M_{\text{virial}} \lesssim 3 \times 10^{15} M_\odot$ (Reiprich & Böhringer 2002) – i.e. well-matched to $10^{15} M_\odot$.

The radius at which the mean enclosed density of a $10^{15} M_\odot$ dark matter halo at the median redshift of the cluster sample ($z = 0.22$) is $\langle \rho(< r) \rangle = 200 \rho_{\text{crit}}$ is $r_{200} = 1.9 \text{ Mpc}$. To ensure that our results are comparable with previous studies of the luminosity gap statistic, data that probe out to $\sim 0.5 r_{200}$ ($\sim 4.5 \text{ arcmin}$) are required. This requirement is met by the Wide-field Infrared Camera (WIRC) on the Hale 200in Telescope at Palomar Observatory (§2.2). Traditionally, the luminosity gap statistic has been studied at optical wavelengths. In contrast, working in the near-infrared permits the use of $(J - K)$ colours as a surrogate for a photometric redshift estimate of cluster galaxies (§3.1), taking advantage of the relative insensitivity of near-infrared colours to spectral type (e.g. Mannucci et al. 2001). This is vital, in the absence of exhaustive spectroscopic catalogs, to weed out non-cluster members when calculating the luminosity gap statistic.

2.2 Ground-based Near-infrared Data

The parent sample of 115 clusters were used as a back-up observing program during observing runs with WIRC (Wilson et al. 2003) on the Hale 200in Telescope¹⁰ during observing runs spanning April

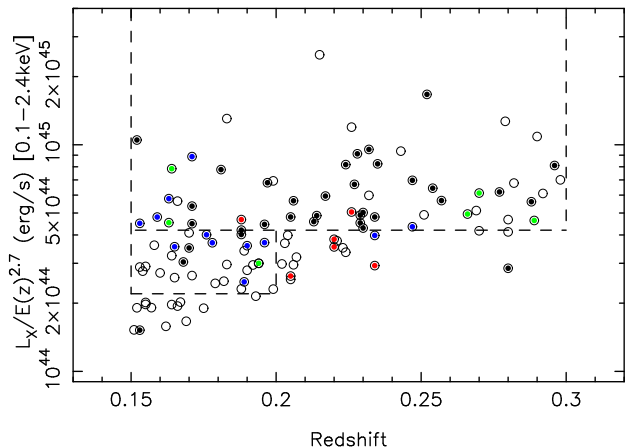


Figure 1. The distribution of the parent sample of 115 clusters in the L_X – redshift plane. Filled data points indicate clusters that we observed in acceptable conditions (see §2.2) with WIRC on the Hale 200-in telescope, and are colour-coded as follows: black – also observed with both *HST* and *Chandra*; blue – also observed with *HST*, but not with *Chandra*; green – also observed with *Chandra*, but not with *HST*; red – observed with neither *HST* nor *Chandra*. Open data points were not observed with WIRC at Palomar, and therefore do not form part of the sample studied in this article. The dashed lines delineate the volume limited samples against which the observed sample is compared statistically in §2.5. The absence of clusters from the parent sample to the lower right is caused by the flux-limit of the ROSAT All-sky Survey.

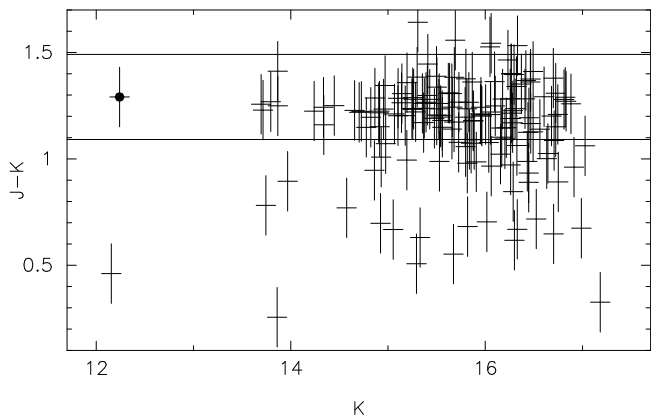


Figure 2. The $(J - K)/K$ colour-magnitude relation for A 1763. The horizontal lines show the region within which likely cluster galaxies were selected. The filled circle denotes the BCG.

2004 to July 2005. Data were acquired when the full width half maximum (FWHM) of point sources exceeded 1 arcsec. In total, data were obtained on 78 clusters, with no pre-selection on cluster properties other than the X-ray selection described above (§2.1). Each cluster was observed with a single $8.7' \times 8.7'$ WIRC pointing. BCGs at $z \simeq 0.2$ have a typical angular extent of $\sim 1 \text{ arcmin}$; the individual exposures were therefore dithered within a box of full-width $80''$ to minimise inclusion of BCG flux in sky-flats constructed from the science data. Each cluster was observed for a total of 600 sec per filter, split into 5 dither positions.

The data were reduced in a uniform and standard manner using an automated pipeline of IRAF tasks to dark subtract, flat-field, align, and co-add the individual frames at the telescope. Data acquired in conditions worse than $\text{FWHM} = 1.5''$ suffered strongly variable transparency and/or non-uniform background, and were

¹⁰ The Hale Telescope at Palomar Observatory is owned and operated by the California Institute of Technology.

Table 1. The observed sample of clusters.

Cluster	α, δ [J2000]	Redshift	$M_{K,BCG}^a$	Δm_{12}^a	HST PID	Also known as
A 68	00 37 05.28 +09 09 10.8	0.255	-26.65	0.25	8249	
A 115	00 55 50.65 +26 24 38.7	0.197	-26.29	0.39	11312	
A 141	01 05 37.17 -24 40 49.7	0.230	-26.54	0.40	10881	RXC J0105.5-2439
ZwCl 0104.4+0048	01 06 49.50 +01 03 22.1	0.255	-26.37	0.52	11312	Z 348
A 209	01 31 53.00 -13 36 34.0	0.206	-26.76	0.87	8249	RXC J0131.8-1336
A 267	01 52 48.72 +01 01 08.4	0.230	-26.56	1.43	8249	RXCJ0152.7+0100
A 291	02 01 43.11 -02 11 48.1	0.196	-25.49	1.79	8301	RXC J0201.7-0212
A 383	02 48 02.00 -03 32 15.0	0.188	-26.24	1.76	8249	RXC J0248.0-0332
RXC J0331.1-2100	03 31 05.87 -21 00 32.7	0.188	-27.07	0.96	10881	
A 521	04 54 06.88 -10 13 24.6	0.247	-26.47	0.00	11312	RXC J0454.1-1014
A 586	07 32 20.42 +31 37 58.8	0.171	-26.31	0.51	8301	
ZwCl 0740.4+1740	07 43 23.16 +17 33 40.0	0.189	-26.26	1.62	11312	Z 1432
A 611	08 00 55.92 +36 03 39.6	0.288	-26.90	1.28	9270	
A 665	08 30 57.36 +65 51 14.4	0.182	-25.81	0.66		
ZwCl 0839.9+2937	08 42 56.06 +29 27 25.7	0.194	-26.45	0.67	11312	Z 1883
ZwCl 0857.9+2107	09 00 36.86 +20 53 40.0	0.235	-25.82	0.34	8301	Z 2089
A 750	09 09 12.74 +10 58 29.1	0.163	-26.52	0.95	11312	
A 773	09 17 54.00 +51 42 57.6	0.217	-26.68	0.47	8249	
ZwCl 0923.6+5340	09 27 10.69 +53 27 30.9	0.205	-25.86	0.55		Z 2379
ZwCl 0949.6+5207	09 52 47.52 +51 53 27.6	0.214	-26.45	1.24	8301	Z 2701
A 901	09 56 26.40 -10 04 12.0	0.163	-25.90	0.08	10395	RXC J0956.4-1004
RX J1000.5+4409	10 00 31.16 +44 08 42.5	0.153	-25.72	0.35	10881	
A 963	10 17 01.20 +39 01 44.4	0.205	-26.42	1.73	8249	
A 1201	11 12 54.61 +13 26 08.2	0.169	-26.25	1.37	8719	
A 1204	11 13 20.55 +17 35 39.1	0.171	-25.80	0.95	8301	
A 1246	11 23 58.83 +21 28 45.4	0.190	-25.92	0.42	8301	RXCJ1123.9+2129
A 1423	11 57 17.43 +33 36 38.6	0.213	-26.16	1.77	8719	
A 1553	12 30 48.95 +10 32 45.6	0.165	-26.82	0.94		
ZwCl 1231.4+1007	12 34 17.45 +09 45 58.1	0.229	-26.21	0.71	8719	Z 5247
A 1634	12 54 01.84 -06 42 14.4	0.196	-25.82	0.61		RXC J1254.0-0642
A 1682	13 06 47.89 +46 33 32.5	0.226	-26.96	0.09	8719	
ZwCl 1309.1+2216	13 11 46.15 +22 01 36.8	0.266	-26.18	2.17		Z 5768
A 1704	13 14 24.38 +64 34 31.0	0.220	-26.34	1.41		
A 1758	13 32 44.47 +50 32 30.5	0.280	-26.26	0.22		
A 1763	13 35 16.32 +40 59 45.6	0.228	-26.84	1.59	8249	
A 1835	14 01 02.40 +02 52 55.2	0.253	-27.32	2.44	8249	
A 1914	14 25 59.78 +37 49 29.1	0.171	-26.62	1.33	8301	
A 1961	14 44 31.85 +31 13 34.3	0.234	-26.47	0.31		
A 1994	14 56 13.48 -05 48 56.6	0.220	-26.45	0.55		RXC J1456.3-0549
MS 1455.0+2232	14 57 15.23 +22 20 34.0	0.258	-26.06	0.11	8301	ZwCl 1454.8+2233, Z7160
A 2009	15 00 19.63 +21 22 08.9	0.153	-25.99	0.17	8301	
ZwCl 1459.4+4240	15 01 23.13 +42 20 39.6	0.290	-26.28	0.07		Z 7215
A 2111	15 39 40.51 +34 25 27.0	0.229	-25.58	0.37		
A 2146	15 56 09.05 +66 21 33.1	0.234	-26.07	0.41	8301	
A 2163	16 15 34.10 -06 07 26.0	0.169	-25.46	0.49		
A 2204	16 32 46.94 +05 34 31.3	0.152	-25.82	0.11	8301	
A 2218	16 35 52.80 +66 12 50.4	0.171	-26.12	0.32	5701	
A 2219	16 40 22.56 +46 42 21.6	0.228	-26.62	1.18	6488	
A 2254	17 17 45.96 +19 40 48.0	0.178	-26.05	0.88	8301	
RX J1720.1+2638	17 20 10.14 +26 37 30.9	0.164	-26.37	1.76	11312	
A 2261	17 22 27.24 +32 07 56.7	0.224	-26.34	2.32	8301	
RXC J2102.1-2431	21 02 09.98 -24 32 01.8	0.188	-26.82	2.04		
A 2345	21 27 13.73 -12 09 46.1	0.176	-26.67	1.09	11312	RXC J2127.1-1209
RX J2129.6+0005	21 29 40.02 +00 05 20.9	0.235	-26.78	1.93	8301	
A 2390	21 53 36.72 +17 41 31.2	0.233	-26.21	1.50	5352	
RXC J2211.7-0350	22 11 45.95 -03 49 45.3	0.270	-26.35	1.71		
A 2485	22 48 31.13 -16 06 25.6	0.247	-26.59	0.00	11312	RXC J2248.5-1606
A 2537	23 08 23.20 -02 11 31.0	0.297	-26.19	0.63	9270	RXC J2308.3-2011
A 2631	23 37 39.82 +00 16 16.9	0.278	-26.35	0.64	11312	RXC J2337.6+0016

^a Uncertainties on $M_{K,BCG}$ and Δm_{12} are dominated by the uncertainties on the photometric calibration, which is ~ 0.1 mag in J- and K-bands.

therefore excluded from the analysis, leaving a total of 59 clusters with good quality data (Table 1). Astrometric and photometric calibration were achieved by reference to the 2MASS catalogs, to root mean square (rms) precisions of 1 arcsec and 0.1 magnitudes respectively (Stott et al. 2008). The results described in this article are insensitive to the uncertainty on the photometric calibration. An example $(J-K)/K$ colour magnitude diagram is shown in Fig. 2. The typical depth reached by the data is $K \simeq 17$; an L^* galaxy has $K \simeq 15$ and a typical BCG has $K \sim 12-13$ at $z \simeq 0.2$.

2.3 Hubble Space Telescope Observations

Hubble Space Telescope (HST)¹¹ imaging data are available through a broad red filter (F606W, F702W, and/or F814W) for 45 of the 59 clusters (Table 1) of which 13 are drawn from new LoCuSS ACS (PID:10881) and WFPC2 (PID:11312) observations. The reduction of the data on 10 clusters observed under PID:5701, PID:6488 and PID:8249 is described by Smith et al. (2005). Of the remaining 36 clusters, the 18 with WFPC2 data (PIDs:5352, 8301, 8719, 11312) were all reduced onto a $0.1''$ pixel scale using WFIXUP, WMOSAIC, IMSHIFT and CRREJ tasks within IRAF to clean, register and combine the individual exposures. Details of the reduction of the remaining clusters observed with ACS are described by Hamilton-Morris et al. (2010, in preparation).

2.4 Chandra X-ray Observations

Chandra X-ray observations are available for 41 of the total sample of 59 clusters. The reduction and analysis of these data are described in detail by Sanderson et al. (2009). In brief, for each cluster, an annular spectral profile was extracted and used to deproject the X-ray emission to measure the gas density and temperature in spherical shells. The phenomenological cluster model of Ascasibar & Diego (2008) was then jointly fitted to the temperature and density profiles to determine the mass profile, assuming hydrostatic equilibrium, following the procedures described in Sanderson & Ponman (2010). The model is based on a Hernquist (1990) density profile, which yields larger scale radii (and correspondingly lower mass concentrations) than the commonly-used NFW profile. Following Sanderson et al. (2009), we also use the logarithmic slope of the gas density profile at $0.04 r_{500}$ (α ; Vikhlinin et al. 2007) as an indicator of cool core strength, which has also been shown to correlate with the substructure fraction of cluster cores, based on strong lens models (Richard et al. 2010b). A more negative value of α indicates a steeper central gas density profile, and thus a stronger cool core, and vice versa.

2.5 Statistical Comparison of Sub-samples

Incomplete coverage of the parent sample of 115 clusters with WIRC, and heterogeneous coverage of the WIRC-observed clusters with other facilities (Fig. 1) may introduce subtle biases into our results. We therefore compare statistically the various observed sub-samples, including for completeness the sub-sample for which *Spitzer* data are available (§3.2). Specifically, the cluster X-ray luminosities are compared, after correction for the modest redshift

Table 2. Statistical Comparison of Sub-samples

Sample	N_{clus}	$\langle \log_{10}(L_X) \rangle^a$
All clusters observed with WIRC	59	44.71 ± 0.03
Clusters observed with WIRC & <i>HST</i>	45	44.71 ± 0.03
Clusters observed with WIRC & <i>Chandra</i>	41	44.76 ± 0.04
Clusters observed with WIRC & <i>Spitzer</i>	39	44.73 ± 0.03
Mean of 100,000 samples drawn randomly from volume-limited sample	59	44.71 ± 0.03

^a The uncertainties are errors on the mean X-ray luminosity of each sample, with the exception of the last row, in which we quote the standard deviation of the 100,000 samples around the mean luminosity of all of these randomly drawn samples.

evolution within the sample due to the expansion of the universe: $L_{X,z} = L_X E(z)^{-2.7}$, where $E(z) = H(z)/H_0 = [\Omega_M(1+z)^3 + \Omega_\Lambda]^{0.5}$ following Evrard et al. (2002).

The mean X-ray luminosity of the full sample of 59 clusters is statistically indistinguishable from the mean luminosity of the sub-samples observed at other wavelengths (Table 2). We also draw 100,000 samples of 59 clusters at random from the combined volume-limited samples defined by $0.15 < z < 0.2$, $2.2 \times 10^{44} \text{ erg s}^{-1} \leq L_{X,z} \leq 4.2 \times 10^{44} \text{ erg s}^{-1}$, and $0.15 < z < 0.3$, $L_{X,z} \geq 4.2 \times 10^{44} \text{ erg s}^{-1}$ (see Fig. 1). The average X-ray luminosity of the observed sample of 59 clusters is well within one standard deviation of the average X-ray luminosity of these randomized samples (Table 2). We therefore conclude that the L_X distributions of the full sample of 59 clusters, the sub-samples observed with other telescopes, and the volume limited-sample defined above, are all statistically indistinguishable from each other. We therefore expect any biases to be negligible, and that our results can be treated as comparable with those that would be achieved with a volume-limited sample. We also take care to double check that the Δm_{12} -distributions of the various observational sub-samples are statistically indistinguishable from each other in §3.

3 ANALYSIS AND RESULTS

3.1 Source Detection and Photometry

The J - and K -band frames were analyzed with SExtractor (Bertin & Arnouts 1996), extracting all objects subtending $> 25 \text{ pixel}$ at $S/N > 2.5 \text{ pixel}^{-1}$. The resulting catalogs were matched using a search radius comparable with the seeing disk, and point sources were excluded based on the stellarity index calculated by SExtractor. In the absence of spectroscopic redshift information we rely on the red ridge line of galaxies seen in the $(J-K)/K$ colour-magnitude diagrams for each cluster (e.g. Fig. 2) to isolate likely cluster galaxies. A simple model based on redshifting local galaxy spectral templates (King & Ellis 1985) confirms that the $(J-K)$ colour of galaxies varies by $\lesssim 0.2 \text{ mag}$ between E/S0 and Scd spectral types. We therefore selected galaxies within ± 0.2 magnitudes of the BCG colour in each cluster as likely cluster members (see horizontal lines in Fig. 2).

The extended envelope of the BCGs typically spans a diameter of $\sim 1 \text{ arcmin}$ in the *HST* frames. In contrast, BCGs typically span just $\sim 20 - 30''$ in the near-infrared frames. The difference is due to the brighter sky in the near-infrared relative to the optical. We therefore use the deep F702W *HST*/WFPC2 data available for 10 clusters in our sample (Smith et al. 2005) to es-

¹¹ Based on observations with the NASA/ESA *Hubble Space Telescope* obtained at the Space Telescope Science Institute, which is operated by the Association of Universities for Research in Astronomy, Inc., under NASA contract NAS 5-26555.

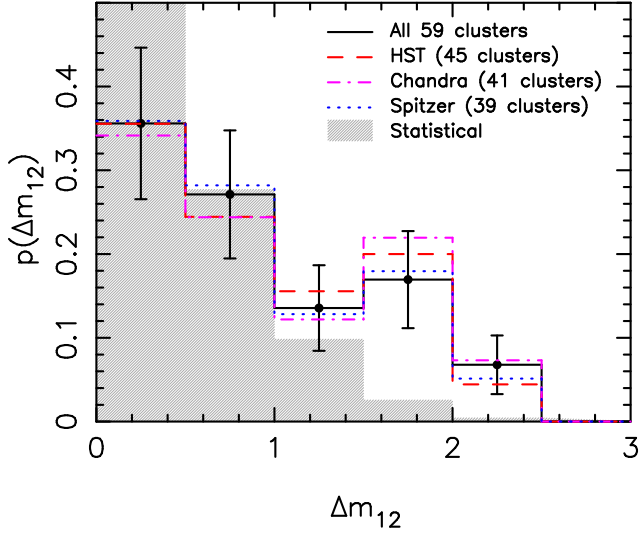


Figure 3. Distribution of the observed luminosity gap (black points and solid line). The gray filled histogram is the expected distribution if the galaxies are drawn at random from a Schechter function following Dariush et al. (2007) (see §3.2 for more details). The dashed, dot-dashed, and dotted histograms show the Δm_{12} -distributions of the sub-samples of clusters for which *HST*, *Chandra*, and *Spitzer* data are available.

timate the K -band flux lost due to the bright K -band sky, under the assumption that the $(R_{702} - K)$ colour of BCGs does not vary significantly with radius on large scales. This assumption introduces negligible systematic uncertainty into our results because colour gradients in elliptical galaxies are measured to be $d(R - K)/d(\log r) \sim 0.3 - 0.4$ (La Barbera et al. 2004, 2010), which translates into a possible ~ 0.1 magnitude systematic error on the factor of 2 radial corrections to the K -band photometry estimated below.

After masking out other galaxies from the data, the BCG R_{702} - and K -band light distributions are modelled using ELLIPSE in the STSDAS package in IRAF. The R_{702} -band model is then used to extrapolate the K -band light distribution out to 2σ above the mean local background. The same procedure was applied to a sample of L^* galaxies detected in the WFPC2 frame of each of these ten clusters. This analysis revealed that reliance on solely K -band data causes the total flux of BCGs to be under-estimated by $\sim 0.3 - 0.7$ mag, with a median of ~ 0.45 mag. This effect is much less severe for non-BCG’s, with total flux being under-estimated by $\sim 0.07 - 0.15$ mag, with a median of 0.1 mag. We fit a straight-line to these data: $\Delta K = \alpha + \beta K$, obtaining $\alpha = -1.67 \pm 0.43$ and $\beta = 0.11 \pm 0.03$. The correction, ΔK , was then applied to all galaxies within our sample. The amplitude of this systematic correction to the luminosity gap statistic measurements is therefore $\beta \Delta m_{12}$ and is typically in the range $\sim 0 - 0.3$ mag with an uncertainty of $\sim 25\%$, both of which are smaller than the bin-width in our subsequent analysis. Our results are therefore not significantly affected by the uncertainties on this correction.

3.2 Luminosity Gap Statistic of $10^{15} M_{\odot}$ Clusters

In the absence of models of the mass distribution, and thus measurements of r_{200} for all clusters in the sample we adopt a fixed projected physical radius of $R = 640$ kpc within which to calculate Δm_{12} for each cluster. This aperture fits comfortably within the observed field of view for all clusters, and corresponds to

$\sim 0.4 r_{200}$ for a $M_{\text{virial}} \simeq 10^{15} M_{\odot}$ cluster at $z = 0.2$. The distribution of the luminosity gap statistic is shown in Fig. 3; $p(\Delta m_{12})$ is a declining function of Δm_{12} . We therefore fit a straight-line to the data: $p(\Delta m_{12}) = A + B \Delta m_{12}$, weighting the data-points by σ^{-2} where σ is the Poisson uncertainty on Δm_{12} in each bin. The best-fit parameter values are: $A = 0.36 \pm 0.03$ and $B = -0.13 \pm 0.02$. We also measure the fraction of “fossil clusters”: a total of 4 clusters have $\Delta m_{12} \geq 2$, yielding a fraction of $10^{15} M_{\odot}$ clusters satisfying this selection of $p(\Delta m_{12} \geq 2) = 0.07_{-0.03}^{+0.05}$, where the error bar is at 1σ using binomial statistics (Gehrels 1986).

Following Dariush et al. (2007) we also show in Fig. 3 the Δm_{12} distribution derived from a Monte Carlo simulation in which galaxies were drawn at random from a Schechter function with $M^* = -24.5$ and $\alpha = -1.2$, adopted from a fit of the Schechter function to the K -band galaxy luminosity function of the Millennium semi-analytic catalogue, and is also consistent with observed luminosity functions (e.g. Lin et al. 2004). This simulation allows us to identify whether the Δm_{12} distribution presents any excess probability over random statistical sampling of a common underlying luminosity function. Excess probability over random is only found at $\Delta m_{12} \gtrsim 1$. We measure the observed probability of a cluster to have a luminosity gap of $\Delta m_{12} \geq 1$ to be $p(\Delta m_{12} \geq 1) = 0.37 \pm 0.08$, compared with the estimated probability based on the Monte Carlo simulation of $p_{\text{MC}}(\Delta m_{12} \geq 1) = 0.13$. We therefore detect an excess probability over random sampling at $\Delta m_{12} \geq 1$ of ~ 0.24 at $\sim 3\sigma$ significance, and conclude that the Δm_{12} distribution at $\Delta m_{12} > 1$ has a physical origin.

The Δm_{12} distributions of the sub-samples of clusters for which *HST*, *Chandra*, and *Spitzer* data are available are statistically consistent with that of the full sample of 59 clusters (Fig. 3). Two sample Kolmogorov-Smirnov (KS) tests that compare the *HST*, *Chandra*, and *Spitzer* sub-samples in turn with the full sample confirm that the probability of the respective sub-samples being drawn from a different underlying Δm_{12} distribution than the full sample is $P \leq 0.1\%$ in all cases, with the largest difference between the cumulative distributions being $D = 0.0748$, between the *Chandra* sub-sample and the full sample.

We also look at how the absolute magnitude of the first and second ranked cluster galaxies vary with Δm_{12} (Fig. 4). The luminosity of the first ranked galaxy increases very slowly with Δm_{12} , remaining in the range $-27 \lesssim M_K \lesssim -26$ across the full range of Δm_{12} . In contrast, the luminosity of the second ranked galaxy declines from $M_K \sim -26$ at $\Delta m_{12} \sim 0$ to $M_K \sim -24$ at $\Delta m_{12} \sim 2$. We characterize these trends by fitting the following relations to the data: $M_{K,1} = \alpha_1 + \beta_1 \Delta m_{12}$ and $M_{K,2} = \alpha_2 + \beta_2 \Delta m_{12}$, where the numerical subscripts denote the first and second ranked galaxies respectively. The best-fit values are: $\alpha_1 = -26.13 \pm 0.02$, $\beta_1 = -0.22 \pm 0.02$, and $\alpha_2 = -26.13 \pm 0.02$, $\beta_2 = 0.78 \pm 0.02$. Empirically large luminosity gap statistics are therefore due to both an over-bright BCG, $M_{K,1}(\Delta m_{12}=2) - M_{K,1}(\Delta m_{12}=0) \simeq -0.4$, and an under-bright second ranked galaxy, $M_{K,2}(\Delta m_{12}=2) - M_{K,2}(\Delta m_{12}=0) \simeq 1.6$. The relative faintness of second ranked galaxies in large luminosity gap clusters supports the idea that the growth of dominant BCGs is driven by the merging of luminous cluster galaxies with the BCG. Indeed the current SFR of BCGs discussed above lends additional support – the BCG in a cluster with a luminosity gap of $\Delta m_{12} = 2$ is $6\times$ more luminous and has a stellar mass of $\sim 10^{11} M_{\odot}$ more than the second ranked galaxy. Just two of the four clusters with $\Delta m_{12} \gtrsim 2$ in Fig. 5 host an active BCG. The most active of these, A 1835, is forming stars at $\text{SFR} = 125 M_{\odot} \text{ yr}^{-1}$ (Egami et al. 2006), and the other, RXJ 2129.6+0005, is forming

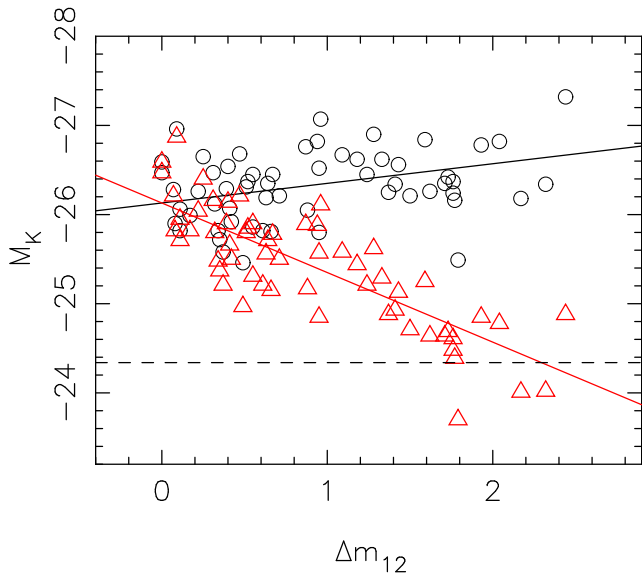


Figure 4. Absolute K -band magnitude of the first (black circles) and second ranked (red triangles) galaxies as a function of luminosity gap. The solid black and red lines show the best-fit straight-line to the data – see §3.2 for more details. The horizontal dashed line is at $M_K = -24.34$, the absolute magnitude of an L^* galaxy, taken from Lin et al. (2004).

stars at $\text{SFR} = 14M_\odot \text{ yr}^{-1}$ (Quillen et al. 2008). These two BCGs would therefore have to form stars continuously at this rate for $\sim 10^9$ and $\sim 10^{10}$ years respectively for their large luminosity gap to be caused exclusively by gas cooling and consequent star formation.

Finally, we note that on average second ranked galaxies in clusters with $\Delta m_{12} > 2$ have $\langle M_{K,2} \rangle = -24.6 \pm 0.6$ where the uncertainty is the rms scatter around the mean. Lin et al. (2004) measured $M_K = -24.34 \pm 0.01$ for L^* cluster galaxies at $z \leq 0.1$, in agreement with similar studies of field galaxies and of higher redshift clusters (De Propris et al. 1999; Cole et al. 2001). The distribution of luminosities of second ranked cluster galaxies in clusters with $\Delta m_{12} > 2$ is therefore statistically consistent with them being L^* galaxies. This contrasts with low mass $\Delta m_{12} > 2$ systems, i.e. fossil groups, in that L^* galaxies are absent from low mass systems. This difference is probably due, at least in part, to the relative inefficiency of galaxy merging in massive clusters.

3.3 Comparing Luminosity Gap with Cool Core Strength

To explore further the physical origin of large luminosity gaps we plot Δm_{12} versus α , the slope of the logarithmic gas density profile at $0.04r_{500}$, for 41 clusters that have also been observed with *Chandra* in Fig. 5. The measurements of α are based on Sanderson et al.’s (2009) analysis of the *Chandra* data (§2.4). At $\Delta m_{12} \simeq 0$ the clusters span the full range of cool core strengths: $-1.2 \lesssim \alpha \lesssim -0.1$. This dynamic range shrinks to just $-1.2 \lesssim \alpha \lesssim -0.6$ at $\Delta m_{12} \gtrsim 2$ – the clusters with large luminosity gaps also host relatively strong cool cores. We also identify star-forming BCGs in Fig. 5. It has long been known that $\text{H}\alpha$ emission from the BCG is closely associated with the presence of significant central cooling in the cluster core (e.g. Heckman 1981; Crawford et al. 1999). More recently, Sanderson et al. (2009) found in their sample of 65 clusters that $\text{H}\alpha$ emitting BCGs occur exclusively in those clusters with the most cuspy inner gas density profiles ($\alpha < -0.85$), and where the projected offset between the

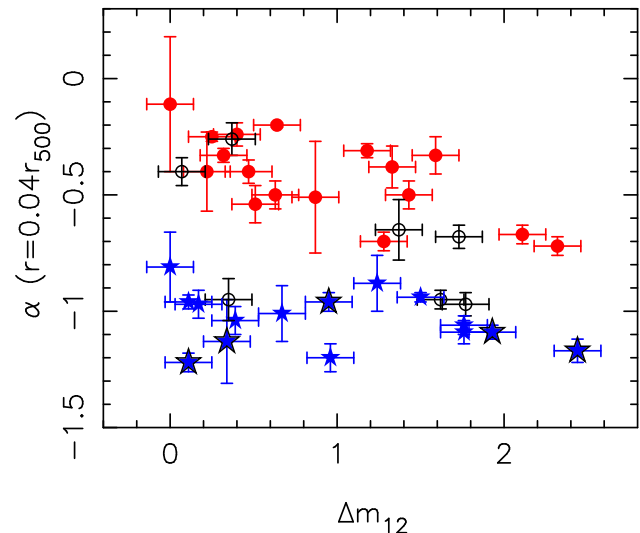


Figure 5. The gradient of the logarithmic gas density profile at $0.04r_{500}$ versus luminosity gap for 41 clusters that have also been observed with *Chandra* and studied by Sanderson et al. (2009). Blue stars correspond to clusters with an $\text{H}\alpha$ emitting BCG (see Sanderson et al. 2009); blue stars with a black outline have also been identified as hosting a BCG that is forming stars at $\text{SFR} \gtrsim 10M_\odot \text{ yr}^{-1}$ using *Spitzer*/MIPS observations; filled red circles denote clusters with BCGs that are not $\text{H}\alpha$ emitters and are forming stars at $\text{SFR} < 10M_\odot \text{ yr}^{-1}$; open black circles indicate clusters that have not been observed with *Spitzer*.

X-ray centroid and the BCG is $\leq 0.02r_{500}$. The same is true of the five BCGs with star formation rates (SFR) of $\gtrsim 10M_\odot \text{ yr}^{-1}$, based on mid-infrared observations with *Spitzer*/MIPS – this SFR corresponds to a flux of $\sim 1\text{mJy}$ from a BCG at $z \simeq 0.2$. These measurements are drawn from the literature (Egami et al. 2006; Quillen et al. 2008) and our own measurements using data from Cycle 4 (PID:40827, PI: Smith; PID: 41011, PI: Egami) the details of which will be published elsewhere (Egami et al., in prep.). Fig. 5 therefore confirms that cool core clusters tend to host actively star-forming BCGs (e.g. Edge et al. 1999; Egami et al. 2006; Quillen et al. 2008). However, cool core clusters ($\alpha \lesssim -1$) with active BCGs (SFR $\gtrsim 10M_\odot \text{ yr}^{-1}$, and/or $\text{H}\alpha$ emission) are found across the full range of Δm_{12} in Fig. 5.

These results are consistent with the interpretation of large luminosity gap clusters as objects that formed relatively early, and subsequently developed a large luminosity gap through the merging of bright cluster galaxies with the BCG. A similarly long period of time – a few Gyr – is required to form a strong cool core following cluster formation. Conversely, if all clusters with smaller luminosity gaps formed more recently than those with larger gaps, and thus have had insufficient time to form a large luminosity gap and a cool core, then they should all host relatively weak cool cores. However this is not the case. This can be understood if the so-called “fossil” status of a large luminosity gap cluster is not the end-point of its evolution. If bright ($L > L^*$) galaxies fall into a cool core “fossil” cluster, then that cluster would move immediately leftward from the bottom right of Fig. 5. As the in-falling system (presumably a group) reaches the cluster core $\sim 1\text{Gyr}$ later, it may disrupt partially or fully the cooling of gas onto the BCG, and cause the cluster to move vertically in the $\Delta m_{12} - \alpha$ plane. This scenario naturally explains the triangular distribution of points in Fig. 5, and is consistent with hierarchical infall (i.e. mergers) playing a role in regulating cooling in cluster cores.

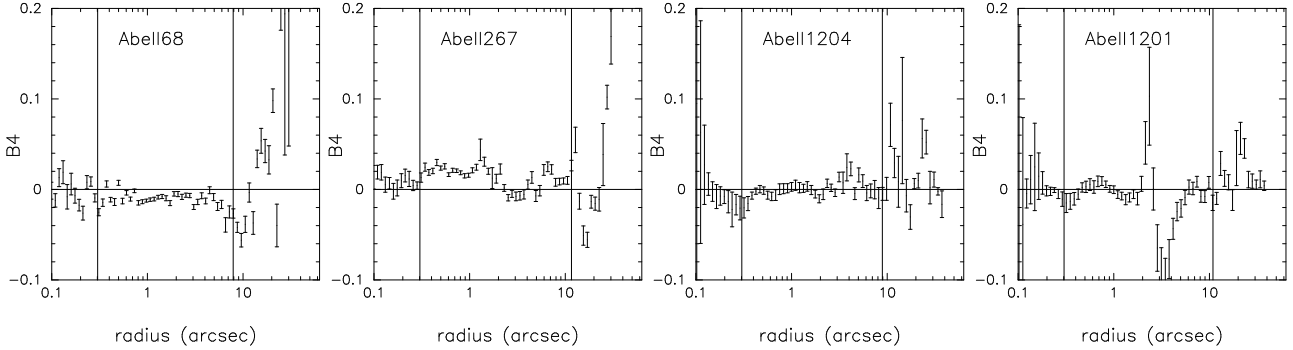


Figure 6. Example isophotal shape profiles. From left to right the BCGs are classified as boxy, disk, pure ellipse and unclassified. The vertical line at the left is set to $3\times$ the FWHM of point sources and the one at the right indicates the half-light radius of the BCG. Note that to keep the analysis simple and conservative, no flux was masked out of the *HST* data. So, for example, the BCG in A 1201 was unclassified because of the impact of the gravitational arc at a BCG-centric radius of $\sim 2''$ (Edge et al. 2003) on the isophotal analysis.

To place this discussion on a more quantitative footing we adopt a strategy that we return to often in §3 – we split the sample into low- ($\Delta m_{12} < 1$) and high- Δm_{12} ($\Delta m_{12} > 1$) sub-samples and perform a two sample KS test on the cumulative distribution of the other variable, in this case α . The hypothesis that high- Δm_{12} clusters are drawn from the same underlying α distribution as low- Δm_{12} clusters is rejected at just 74% confidence, i.e. slightly over 1σ significance, based on a maximum difference between the cumulative α distributions of $D = 0.3102$. In the absence of a decisive test, we therefore divide the sample at $\Delta m_{12} = 1.5$, i.e. a more extreme value of Δm_{12} , attempting to identify roughly the luminosity gap at which the α distribution diverges from that of lower- Δm_{12} clusters. This time the two sample KS test rejects the null hypothesis at 95% confidence – i.e. 2σ – based on a maximum difference between the respective cumulative α distributions of $D = 0.472$.

3.4 Comparing the Luminosity Gap with BCG Morphology

We use the high angular resolution *HST* imaging observations of the 45 clusters discussed in §2.3 to measure the isophotal shape of the BCGs in these clusters. The ELLIPSE task in IRAF was used to measure the fourth Fourier coefficient (B_4) of the light distribution. This coefficient indicates whether the galaxy has a disk or boxy shape (Bender 1988). In Fig. 6 we show the B_4 profile of four BCGs to illustrate the diversity within the sample. Following Bender et al. (1989) we tried to use the extremum value of B_4 (i.e. $B_{4,\text{ext}}$ in Table 3) to classify galaxies as either disk ($B_{4,\text{ext}} > 0$) or boxy ($B_{4,\text{ext}} < 0$). If the B_4 profile passes through a stationary point, then the extremum is obtained by finding the maximum or minimum value of B_4 in the radial range enclosed by $3\times$ the FWHM of point sources and the effective radius derived from a de Vaucouleurs profile fit. In the absence of a stationary point, the extremum value of B_4 is the value at the effective radius, under the assumption that B_4 is a monotonic function of radius. However B_4 is in general not a monotonic function of radius for BCGs in our sample, even for those with isophotes that have, on average, boxy and disk isophotes (Fig. 6). For these reasons, the isophotal shapes of 22 out of 45 BCGs cannot be classified based on $B_{4,\text{ext}}$. We also find some clusters (e.g. A 1204 – see Fig. 6) in which B_4 is consistent with zero across the full radial range of the data.

We therefore implement a modified scheme, in which we calculate the error-weighted mean value of B_4 in the same radial range

as above, with no weighting of the bins to account for the variation of the bin solid angle as a function of radius. BCGs with $\langle B_4 \rangle$ consistent with zero within the uncertainties were classified as elliptical, otherwise BCGs are classified as Boxy or Disky if $\langle B_4 \rangle < 0$ or $\langle B_4 \rangle > 0$ respectively. Finally, a BCG is “Unclassified” if the error on $\langle B_4 \rangle$ is comparable with the dynamic range of the data, i.e. ≥ 0.01 . BCG morphologies derived under both Bender et al.’s “extremum” scheme and our own “mean” scheme are listed in Table 3 along with the Boxy/Disky/Elliptical/Unclassified classification based on each method. The respective methods agree on morphological classification for 16 of the 22 BCGs for which classification was possible under both methods. However, only three of the six discrepant BCGs have $\langle B_4 \rangle$ and $B_{4,\text{ext}}$ values that formally disagree between the methods within the quoted uncertainties – A 521, A 750 and ZwCl 0949.6+5207. The important advantage of our method is that classification is possible for an additional 15 BCGs that were unclassifiable under the Bender et al. scheme. We therefore adopt $\langle B_4 \rangle$ as our measure of BCG morphology for all clusters with *HST* data for the reasons outlined above regarding the general absence of clearly defined stationary points and monotonic behaviour of the B_4 profiles.

In summary, out of 45 clusters, 10 are classified as Boxy, 13 as Disky, 14 as Elliptical, and 8 are Unclassified. In Fig 7 we plot $\langle B_4 \rangle$ versus Δm_{12} , the most striking feature of which is the lack of clusters with large Δm_{12} and negative $\langle B_4 \rangle$, i.e. boxy BCGs appear not to live in large luminosity gap clusters. As in §3.3, we split the clusters into low- Δm_{12} ($\Delta m_{12} \leq 1$) and high- Δm_{12} ($\Delta m_{12} > 1$) samples and perform a two-sample KS test. The low- and high- Δm_{12} samples contain 27 and 18 clusters respectively, with a maximum difference between their cumulative $\langle B_4 \rangle$ -distributions of $D = 0.3567$. The hypothesis that the low- and high- Δm_{12} samples are drawn from the same underlying $\langle B_4 \rangle$ distribution is therefore disfavoured at 91% confidence, i.e. 1.7σ . Unlike the situation for the analysis of the α distributions of high- and low- Δm_{12} clusters in §3.3, the significance with which the null hypothesis is rejected does not increase if the sub-samples are re-defined by splitting the full sample at $\Delta m_{12} = 1.5$. This is obvious from a comparison of Figs. 5 & 7, and suggests that the relationship between Δm_{12} and BCG morphology is stronger than between Δm_{12} and cool core strength.

Table 3. Results from Isophotal Analysis of Brightest Cluster Galaxies using *HST* data.

Cluster	Effective radius (arcsec)	Extremum Method $100B_{4,ext}$	Method Classification	Mean Method $100 \langle B_4 \rangle$	Method Classification
A 68	7.9	-2.0±0.4	Boxy	-0.99±0.19	Boxy
A 115	4.1	...	Unclassified	+0.96±0.22	Disky
A 141	3.6	+3.4±0.9	Disky	+1.09±0.19	Disky
ZwCl0104.4+0048	4.1	...	Unclassified	-0.14±0.80	Elliptical
A 209	7.4	+1.8±0.5	Disky	+0.45±0.07	Disky
A 267	11.6	+3.5±1.2	Disky	+0.99±0.17	Disky
A 291	7.3	+2.1±0.6	Disky	+0.67±0.24	Disky
A 383	8.3	...	Unclassified	-0.20±0.97	Unclassified
RXC J0331.1-2100	3.1	...	Unclassified	-2.69±7.50	Unclassified
A 521	3.9	-3.1±1.0	Boxy	-0.44±0.79	Elliptical
A 586	7.7	...	Unclassified	-0.16±0.64	Elliptical
ZwCl0740+1740	5.5	+0.1±0.2	Elliptical	-0.11±0.06	Boxy
A 611	3.5	...	Unclassified	-0.21±0.15	Boxy
ZwCl0839.9+2937	3.5	...	Unclassified	+0.84±0.50	Disky
ZwCl0857.9+2107	4.6	-4.0±1.1	Boxy	-1.49±0.61	Boxy
A 750	4.0	+5.0±1.5	Disky	+0.11±1.45	Unclassified
A 773	6.8	-2.1±0.4	Boxy	-0.50±0.18	Boxy
ZwCl0949.6+5207	7.1	+2.4±0.7	Disky	+0.22±0.30	Elliptical
A 901	3.2	+1.1±0.3	Disky	+0.50±0.10	Disky
RX J1000.5+4409	3.1	...	Unclassified	-0.77±0.18	Boxy
A 963	14.3	...	Unclassified	+0.46±0.19	Disky
A 1201	10.8	...	Unclassified	-0.26±0.48	Elliptical
A 1204	8.9	0.0±0.7	Elliptical	-0.10±0.21	Elliptical
A 1246	8.6	...	Unclassified	-0.14±1.78	Unclassified
A 1423	7.4	...	Unclassified	-0.91±60.6	Unclassified
ZwCl1231.4+1007	4.4	-1.3±0.5	Boxy	-0.56±0.19	Boxy
A 1682	6.2	0.0±0.5	Elliptical	-0.43±0.27	Boxy
A 1763	8.2	0.0±0.6	Elliptical	+0.04±0.08	Elliptical
A 1835	6.8	...	Unclassified	+1.10±0.60	Disky
A 1914	12.2	0.0±0.5	Elliptical	+0.25±0.15	Disky
MS 1455.0+2232	5.0	...	Unclassified	-0.47±0.25	Boxy
A 2009	9.3	...	Unclassified	+0.14±0.19	Elliptical
A 2146	6.3	...	Unclassified	-0.20±0.50	Elliptical
A 2204	7.9	...	Unclassified	+0.08±1.20	Unclassified
A 2218	8.1	+2.3±0.8	Disky	+0.83±0.29	Disky
A 2219	8.5	...	Unclassified	+0.83±0.19	Disky
A 2254	9.6	...	Unclassified	-0.03±0.36	Elliptical
RXJ 1720.1-2638	5.5	...	Unclassified	+0.28±1.39	Unclassified
A 2261	7.2	...	Unclassified	+0.39±7.20	Unclassified
A 2345	7.8	0.0±0.5	Elliptical	+0.03±0.09	Elliptical
RX J2129.6+0005	9.6	...	Unclassified	-0.16±0.60	Elliptical
A 2390	3.5	+3.5±0.5	Disky	+1.42±0.32	Disky
A 2485	3.9	-0.5±0.6	Elliptical	+0.19±0.63	Elliptical
A 2537	5.2	0.0±0.3	Elliptical	-0.11±0.18	Elliptical
A 2631	6.0	0.0±0.5	Elliptical	-0.24±0.12	Boxy

3.5 Comparing the Luminosity Gap with Cluster Concentration

To investigate the possibility that high- Δm_{12} clusters formed at earlier times than low- Δm_{12} clusters, we explore the relationship between Δm_{12} and the shape of the cluster dark matter halos via the concentration parameter. In Fig. 8 we plot Δm_{12} versus concentration, c_{500} for the 41 clusters with available *Chandra* data Sanderson et al. (2009) (§2.4). The $c_{500} - \Delta m_{12}$ distribution is similar to the $\langle B_4 \rangle - \Delta m_{12}$ distribution in that the lower-right of both plots is empty, and that clusters with $\Delta m_{12} < 1$ span the full dynamic range in the vertical axis. To quantify this we again perform a two sample KS test, on the $\Delta m_{12} < 1$ and $\Delta m_{12} > 1$

sub-samples. In this case the low- and high- Δm_{12} samples contain 24 and 17 clusters respectively, with a maximum difference between their cumulative c_{500} -distributions of $D = 0.2574$. Acceptance/rejection of the null hypothesis that low- and high- Δm_{12} clusters are drawn from same underlying c_{500} -distribution therefore have roughly equal probability. However if we modify the definition of the low- and high- Δm_{12} sub-samples by splitting the full sample at $\Delta m_{12} = 1.5$ we are able to reject the null hypothesis at $\sim 1.7\sigma$. We therefore conclude that the $c_{500} - \Delta m_{12}$ plane qualitatively supports the interpretation of the $\langle B_4 \rangle - \Delta m_{12}$ plane, however statistically this is not decisive. Specifically, clusters with a large luminosity gap tend to have a relatively large concentration parameter, although there is a curious deficit of clusters with

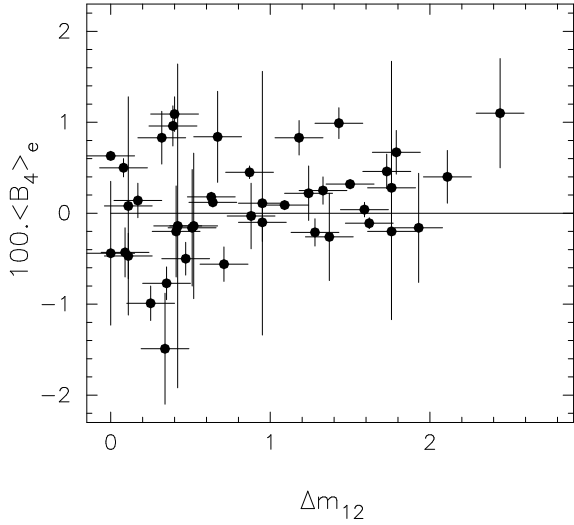


Figure 7. Luminosity gap statistic (Δm_{12}) versus error-weighted mean fourth Fourier component of the BCG light distribution ($\langle B_4 \rangle$). Positive values of $\langle B_4 \rangle$ correspond to Disky BCGs; negative values correspond to Boxy BCGs; values consistent with zero are consistent with elliptical isophotes. Clusters with $\Delta m_{12} \lesssim 1$ host BCGs with both Boxy and Disky isophotes. In contrast clusters with $\Delta m_{12} \gtrsim 1$ host only non-Boxy (i.e. Elliptical or Disky BCGs).

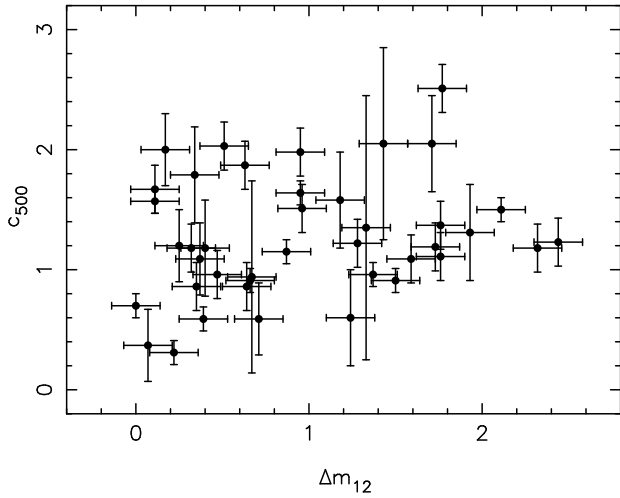


Figure 8. Concentration c_{500} versus luminosity gap for 41 clusters for which the X-ray-based mass profiles are available from Sanderson et al.’s (2009) analysis of archival *Chandra* data.

$\Delta m_{12} \gtrsim 1.8$ and $c_{500} \gtrsim 1.5$. Clusters with lower luminosity gaps plausibly comprise both clusters that formed more recently than clusters with large gaps – and thus have lower concentration parameters – and clusters that used to have a large luminosity gap, and thus formed early, and have a higher concentration parameter, but that then suffered infall of bright ($L > L^*$) galaxies. Put another way, the existence of clusters in the top left corner of Fig. 8 is consistent with the timescale on which the concentration parameter of a cluster may be reset following a cluster-cluster merger being long compared with the infall timescale of ~ 1 Gyr.

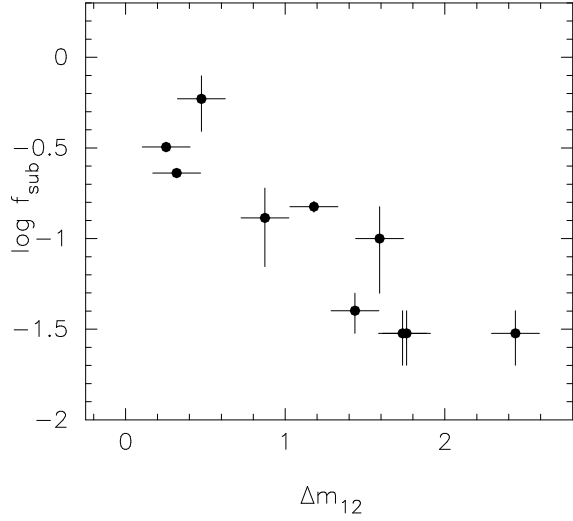


Figure 9. Luminosity gap versus substructure fraction measured within $R \leq 250h^{-1}$ kpc in 10 clusters from our sample by Smith et al. (2005).

3.6 Comparing the Luminosity Gap with Cluster Substructure

Measurements of the substructure fraction (f_{sub}), i.e. the fraction of the total cluster mass that resides in substructures, are available for ten of the clusters (Smith et al. 2005) from our sample of 59. Smith et al.’s gravitational lens models include mass components that account explicitly for substructures required to reproduce the observed positions of multiply-imaged background galaxies – these substructures comprise both galaxy group and individual galaxy masses. We plot f_{sub} versus Δm_{12} for these ten clusters in Fig. 9, revealing a relationship between these quantities in the sense that clusters with simpler gravitational potentials (low f_{sub}) have more dominant BCGs (high Δm_{12}), and vice versa. To quantify this relationship, we fit a simple model to the data: $\log f_{\text{sub}} = \mu + \nu \Delta m_{12}$, and obtain best-fit parameters of: $\mu = -0.29 \pm 0.15$ and $\nu = -0.58 \pm 0.11$. This result is consistent with that found by Richard et al. (2010b), despite the smaller aperture of 250kpc used in their study. This consistency arises because the typical projected separation of the first and second ranked galaxies in our sample is $\lesssim 250$ kpc. We also double-check that the Δm_{12} distribution of the 10 clusters in Fig. 9 is consistent with that of the full sample, finding a maximum difference between the cumulative Δm_{12} distributions of $D = 0.2414$, indicating roughly equal probability of rejection/acceptance of the hypothesis that the two samples are drawn from different underlying populations.

3.7 Summary

We now summarize the comparison of our luminosity gap measurements with other probes of the structure, and thus the age and assembly history of clusters, and discuss the interpretation of these results.

The clearest empirical relationship found is between the Δm_{12} and f_{sub} in the sense that clusters with a dominant BCG ($\Delta m_{12} > 1$) have a lower substructure fraction ($f_{\text{sub}} < 0.1$) and vice versa. The strong correlation between Δm_{12} and f_{sub} is in stark contrast with the triangular distributions of clusters in the Δm_{12} - α , Δm_{12} - $\langle B_4 \rangle$, and Δm_{12} - c_{500} planes. A simple physical interpretation of the Δm_{12} - f_{sub} relation is that both quantities

are sensitive to the same thing. As galaxies and groups of galaxies fall into clusters the light emitted by the galaxies will either cause Δm_{12} to decrease or stay the same, depending on how bright the infalling galaxies are. At the same time the total mass of these galaxies and the group-scale halos within which they may be embedded causes f_{sub} to increase. Early studies discussed the idea that galaxy groups with $\Delta m_{12} \geq 2$ may have formed at earlier times than groups with $\Delta m_{12} < 2$. However, more recently, a variety of studies have shown that both Δm_{12} and f_{sub} are correlated with *both* the formation epoch of the host dark matter halo, *and* the recent hierarchical assembly history of the halo (Dariush et al. 2007, 2010; Smith & Taylor 2008). Therefore both theoretical and observational studies across a broad range of dark matter halo mass are converging on the view that “fossil” status is not an end-point in the evolution of galaxy systems that formed early. Rather it is a phase that a galaxy system can evolve through if it formed early and then suffered minimal hierarchical infall after the formation of a bright massive central galaxy. The triangular distribution of clusters in the Δm_{12} - α , Δm_{12} - $\langle B_4 \rangle$, and Δm_{12} - c_{500} planes are all consistent with this interpretation, and inconsistent with the idea that fossil galaxy systems are evolutionary cul-de-sacs. Specifically, if a cluster forms early and then sufficient time elapses for a large luminosity gap to form via merging of L^* gas-rich galaxies to form the BCG, and for a cool core to form, then this cluster will reside in the top-right corner of Figs. 7 & 8 and the bottom right of Fig. 5. If a $\gtrsim L^*$ galaxy then falls into the cluster, either on its own or in a group, then the cluster would move left-ward in all of Figs 5, 7, and 8 as soon as the infalling galaxy system crosses the aperture within which Δm_{12} is measured (in our case $0.4r_{200}$). Several Gyr later the infalling structure will reach the center of the cluster, and its merger with the cluster may be sufficiently energetic to modify the strength of the cluster cool core, the shape of the BCG, and the concentration of the cluster dark matter halo. In this way, clusters can move vertically in Figs. 5, 7, and 8, and produce the observed triangular distribution of clusters.

The interpretation of non-boxy morphologies ($\langle B_4 \rangle \geq 0$) of BCGs in clusters with large luminosity gaps is an important element of the discussion above. Khochfar & Burkert (2005) showed that the morphology of early-type galaxies is sensitive to the morphology (indicative of gas content) of their progenitors and subsequent gas infall. The straightforward interpretation of the observables is therefore that dominant BCGs formed from mergers of gas rich (presumably spiral) galaxies and/or have accreted gas since the last major merger in their assembly history. Formation of dominant BCGs from gas rich progenitors is consistent with the early formation of these BCGs as discussed above, because at earlier times the galaxies from which BCGs formed would have been more gas rich than at later times.

To disentangle the relative contribution of gas rich mergers and accretion of gas to the disk shape of some BCGs we plot in Fig. 10 α , the slope of the logarithmic gas density profile at $0.04r_{500}$ versus $\langle B_4 \rangle$. If BCG morphology is strongly influenced by gas cooling onto the BCG then one would expect a relationship between α and $\langle B_4 \rangle$ in the sense that disk BCGs ($\langle B_4 \rangle > 1$) would live in clusters with a steep central ($\alpha < -0.5$) gas density profile. This is because clusters with steep central gas density profiles host a cool core – i.e. a central positive temperature gradient, absence of an entropy core, and a cooling timescale short compared with the age of the universe. However we do not find any strong relationship between $\langle B_4 \rangle$ and α in Fig. 10. We divide the 41 clusters with *Chandra* data into those with the strongest cool cores – $\alpha < -0.9$ – and the rest. A two sample KS test on these

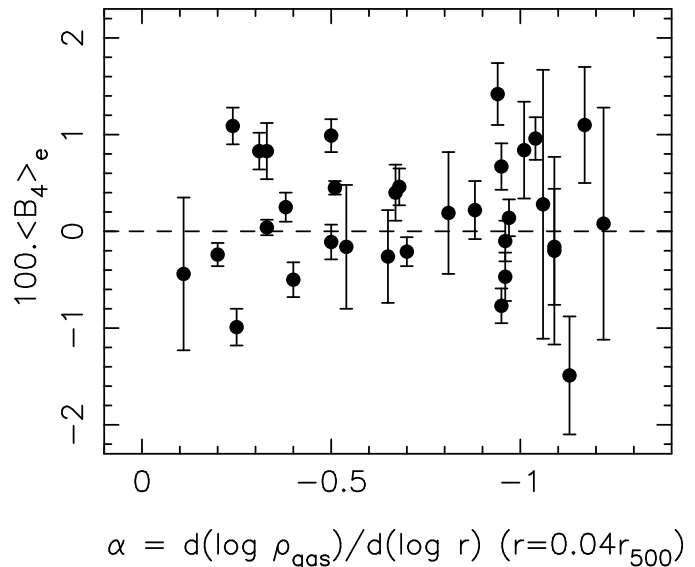


Figure 10. Strength of the cool core in each cluster, as measured by α the slope of the logarithmic gas density profile at $0.04r_{500}$ from Sanderson et al. (2009) versus the $\langle B_4 \rangle$. The absence of a relationship between α and $\langle B_4 \rangle$ suggests that disk BCG isophotes are more likely caused by such BCGs being formed from mergers between gas rich galaxies than by cooling of gas onto the BCG. The typical error bar on α is $\lesssim 0.1$.

two sub-samples yields a maximum difference between the cumulative $\langle B_4 \rangle$ -distributions of $D = 0.209$, indicating roughly equal probability of accepting/rejecting the hypothesis that the two distributions are drawn from the same underlying distributions.

In the absence of a strong relationship between cool core strength and BCG morphology, we therefore conclude that BCG morphology is more sensitive to the gas content of the galaxies that merged to form it, than to the subsequent gas accretion history of the BCG. This view is consistent with the comparison of α , Δm_{12} and BCG activity in Fig. 5 and the discussion of the dependence of $M_{K,2}$ on Δm_{12} in §3.2. The key point being that the merging of luminous cluster galaxies to form the BCG appears to have a much stronger influence on luminosity gap than gas cooling and subsequent star formation within BCGs.

4 COMPARISON WITH THEORETICAL PREDICTIONS

Modern galaxy formation and evolution models contain physical prescriptions for many physical processes relevant to the formation and evolution of galaxies, including dynamical friction, conversion of cold gas into stars during galaxy mergers, and AGN feedback. These processes are particularly important in the centres of galaxy clusters where they regulate the cooling of gas onto the most massive galaxies in the universe – BCGs. However the models were not constrained by the luminosity gap distribution; our observational results can therefore provide a strong test of the models.

We compare our observations with the Bower et al. (2006), Croton et al. (2006), and de Lucia & Blaizot (2007) semi-analytic models, all of which are based on the Millennium Simulation¹² – a cosmological numerical simulation of dark matter in a volume

¹² The Millennium Simulation used in this paper was carried out by the Virgo Supercomputing Consortium at the Computing Centre of the Max-

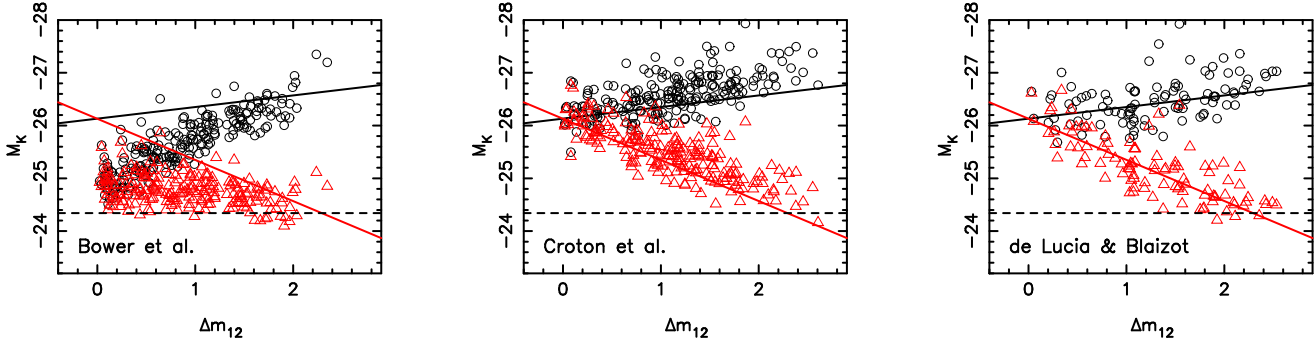


Figure 12. Absolute K -band magnitude of the first (black circles) and second ranked (red triangles) galaxies as a function of luminosity gap from the three semi-analytic galaxy formation models discussed in §4. The solid black and red lines show the best straight-line fit to the observational data shown in Fig. 4. The horizontal dashed line in each panel is at $M_K = -24.34$, the absolute magnitude of an L^* galaxy, taken from Lin et al. (2004).

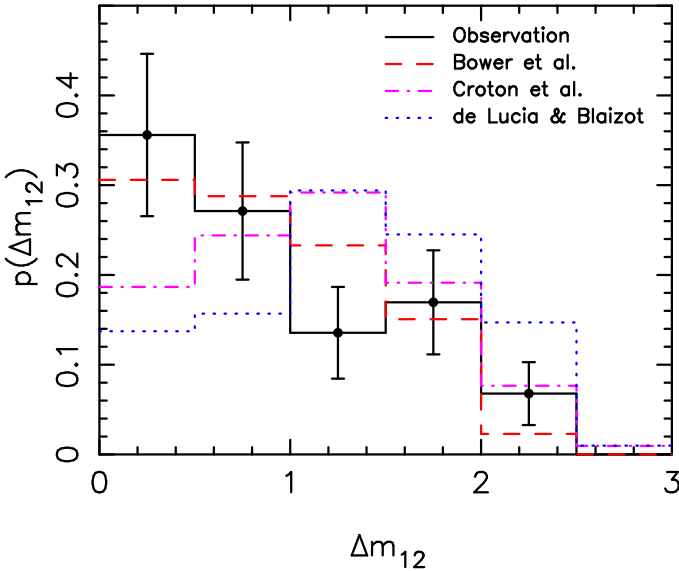


Figure 11. Distribution of the observed luminosity gap (black points – see also Fig. 3) compared with the same for clusters with $M_{\text{virial}} \geq 5 \times 10^{14} M_{\odot}$, measured within a projected BCG-centric radius of 640kpc using the the Millennium simulation-based semi-analytic galaxy formation models of Bower et al. (2006), Croton et al. (2006), and de Lucia & Blaizot (2007). The error bar on each bin in the theoretical histograms is comparable with the observational errors.

spanning $500h^{-1}\text{Mpc}$ containing $\sim 10^{10}$ particles. An important difference between the models is that the Bower et al. model implements “quasar” mode AGN feedback, whereas the Croton et al. and de Lucia & Blaizot models implement “radio” mode AGN feedback. We also note that de Lucia & Blaizot compared their model predictions with the observed properties of BCGs, however they didn’t compare with observed luminosity gaps.

First we select dark matter halos from the Millennium dark matter friends of friends catalogue. Within the whole simulated volume, 209 haloes were found with masses greater than $5 \times 10^{14} M_{\odot}$, i.e. above the mass threshold of the observed sample. We then extracted galaxies in these 209 halos from the semi-analytic galaxy catalogues based on each of the three models. The K -band luminosity gap was computed for each halo within a projected cluster-

centric radius of 640kpc. The predicted luminosity gap statistic distributions are over-plotted on the observed distribution in Fig 11.

The observed Δm_{12} distribution is consistent, within the uncertainties with a monotonically declining function of Δm_{12} (§3.2). The Bower et al. model matches this observational result well, and the predicted fraction of clusters with the most extreme luminosity gaps is $p(\Delta m_{12} \geq 2) = 0.02^{+0.02}_{-0.01}$, just $\sim 1.3\sigma$ below the observed fraction of $p(\Delta m_{12} \geq 2) = 0.07^{+0.05}_{-0.03}$ (§3.2). In contrast, the Croton et al. model peaks at $\Delta m_{12} \sim 1 - 1.5$ – i.e. it does not predict a monotonic decline of $p(\Delta m_{12})$ – however it predicts $p(\Delta m_{12} \geq 2) = 8.6^{+2.4}_{-2.0}\%$ which is in excellent agreement with the observations. The de Lucia & Blaizot model predicts a yet more prominent peak at $\Delta m_{12} \sim 1 - 1.5$, and a yet higher fraction of clusters with extreme Δm_{12} , $P(\Delta m_{12} \geq 2) = 16.7^{+4.5}_{-3.8}\%$, that disagrees with the observations at $\sim 2\sigma$.

Following the same approach as in §3.2, we also decompose the predicted Δm_{12} distributions into the predicted absolute magnitudes of the first ($M_{K,1}$) and second ($M_{K,2}$) ranked galaxies (Fig. 12). The most striking feature of this figure is that the slopes of $M_{K,1}$ versus Δm_{12} and $M_{K,2}$ versus Δm_{12} are much steeper and shallower than the observations respectively in the Bower et al. model. In contrast, the Croton et al. and de Lucia & Blaizot models succeed much better in reproducing the observed trends. Interestingly, the discrepant trends in $M_{K,1} - \Delta m_{12}$ and $M_{K,2} - \Delta m_{12}$ within the Bower et al. model conspire to produce a distribution of Δm_{12} in Fig. 3 that is in good agreement with observations.

The absolute magnitudes of BCGs span $\sim 2\text{mag}$ in the Bower et al. model, in contrast to the observed range of $\sim 1\text{mag}$. As BCGs grow, the largest increase in luminosity from purely ingesting another galaxy is a brightening by 0.75mag, i.e. a merger between the brightest two galaxies in a cluster with $\Delta m_{12} = 0$. The very large spread in M_K for BCGs in the Bower et al. model therefore indicates that the conversion of cold gas into stars is too efficient in their model. In the model, most of the mergers that form BCGs are between gas poor galaxies. The main source of gas for formation of new stars is that which cools from the intracluster medium. The steep relationship between $M_{K,1}$ and Δm_{12} therefore implies that AGN feedback in BCGs is too weak in the Bower et al. model. An important caveat on this interpretation is that we showed in §§3.4 & 3.7 that clusters with large luminosity gaps ($\Delta m_{12} \geq 1$) have non-boxy isophotes and therefore likely formed from mergers of gas rich galaxies, i.e. probably at higher redshift than the BCGs in the model.

The shallow slope of the relationship between $M_{K,2}$ and Δm_{12} in the Bower et al. model implies that the replenishment of

the supply of cluster galaxies that are ingested into their respective BCGs is too efficient in this model. Specifically, the difference in slopes of $M_{K,2} - \Delta m_{12}$ between Bower et al. and the other two models could arise from differing treatments of the merging of galaxies in the respective models following the time at which individual galaxy halos lose their identity following ingestion into the parent cluster halo. We also comment, more generally, that the galaxies in Bower et al.'s model tend to be less luminous than the observed galaxies by ~ 0.5 mag, and those in Croton et al.'s model tend to be over-luminous by ~ 0.3 mag. This suggests that the strength of feedback in the general cluster population may be too strong in the former and too weak in the latter model.

For completeness, we also compare our measurement of the fraction of $10^{15} M_{\odot}$ clusters that satisfy $\Delta m_{12} \geq 2$ with predictions from Milosavljević et al.'s (2006) analytic model. Our measurement of $0.07_{-0.03}^{+0.05}$ is well within 2σ of Milosavljević et al.'s prediction of 0.03. The most obvious difference between their model and our observations is that the prediction is calculated within the cluster virial radii, in contrast to our calculation within a projected cluster-centric radius of $\sim 0.4r_{200}$. The larger volume within each cluster probed by Milosavljević et al. will reduce the probability of finding clusters with large luminosity gap statistics. The same authors also estimate the fraction of $10^{15} M_{\odot}$ clusters with $\Delta m_{12} \geq 2$ using data from the Sloan Digital Sky Survey (Miller et al. 2005), obtaining a similar fraction to their prediction. The possible disagreement between this estimate and our own is harder to understand because both use a similar physical aperture for the calculation of Δm_{12} . We note, however, that the two observed cluster samples are selected in different ways; our sample is X-ray selected whilst SDSS is optically selected.

5 CONCLUSIONS

We have combined wide-field near-infrared imaging from the WIRC camera on the Hale 200in telescope, with *HST*, *Chandra*, and *Spitzer* observations of 59 massive galaxy clusters at $z \simeq 0.2$ to explore the connections between the formation histories of BCGs and the galaxy clusters that they inhabit. This large statistical sample is intended to be representative of the underlying population of massive X-ray luminous clusters. Extensive tests confirm that results based on this sample can be regarded as statistically compatible with those from a complete volume-limited sample. Our main empirical results are as follows:

(i) We have made the first observational measurement of the distribution of the luminosity gap statistic, Δm_{12} , of massive $\sim 10^{15} M_{\odot}$ clusters. The probability distribution of the luminosity gap statistic is a monotonically declining function of Δm_{12} , well described by the relation $p(\Delta m_{12}) = A + B\Delta m_{12}$ with $A = 0.41 \pm 0.03$ and $B = -0.13 \pm 0.02$.

(ii) Following Dariush et al. (2007) we used Monte Carlo simulations to quantify the fraction of clusters with large luminosity gaps expected from random sampling of a Schechter function. The observed distribution exceeds the statistical distribution derived from the Monte Carlo simulation at $\Delta m_{12} \geq 1$ at $\sim 3\sigma$ significance, confirming that the most extreme luminosity gaps have a physical origin, and are not statistical flukes.

(iii) Four of our sample of 59 clusters have extreme luminosity gaps of $\Delta m_{12} \geq 2$ – ZwCl 1309.1+2216, A 1835, A 2261, and RXC J2102.1–2431 – which equates to a fraction of $10^{15} M_{\odot}$ clusters that have $\Delta m_{12} \geq 2$ of $p(\Delta m_{12} \geq 2) = 0.07_{-0.03}^{+0.05}$.

(iv) The morphology of 45/59 BCGs was measured by analyzing the shape of the BCG isophotes in archival and new *HST* observations of the cluster cores. The split between boxy, elliptical and disk isophotes is: 22% boxy, 32% elliptical, 29% disk, with 17% unclassified.

(v) A strong correlation is found between Δm_{12} and f_{sub} , the fraction of mass in the cluster cores associated with group- and galaxy scale dark matter halos, the latter coming from published gravitational lens models of the cluster cores (Smith et al. 2005). The relationship between Δm_{12} and f_{sub} is parameterized thus: $\log f_{\text{sub}} = \mu + \nu \Delta m_{12}$, with best fit parameters $\mu = -0.29 \pm 0.15$ and $\nu = -0.58 \pm 0.11$.

(vi) Clusters with large luminosity gaps, $\Delta m_{12} \gtrsim 1 - 1.5$, have cuspy gas density profiles, and thus relatively strong cool cores ($\alpha \leq -0.6$, where α is the logarithmic gas density profiles at $0.04r_{500}$), elliptical or disk BCGs ($\langle B_4 \rangle \geq 0$, where B_4 is the fourth-order Fourier co-efficient of the optical isophotes), concentrated dark matter density profiles ($c_{500} \gtrsim 1$, where c_{500} is based on a Hernquist 1990 model fit to the *Chandra* data), and small substructure fraction ($f_{\text{sub}} \lesssim 0.1$, where f_{sub} is based on strong lens modeling of the mass distribution).

(vii) In contrast, clusters with small luminosity gaps, $\Delta m_{12} \lesssim 1$, span the full range of observed cool core strengths ($-1.3 \lesssim \alpha \lesssim 0$), span the full range of boxy, elliptical, and disk BCG morphologies ($-0.015 \lesssim \langle B_4 \rangle \lesssim -0.015$), span the full range of concentrations ($c_{500} \sim 0 - 2.5$), and have large substructure fractions ($f_{\text{sub}} \gtrsim 0.1$).

Clusters with $\Delta m_{12} \gtrsim 1$ are therefore a more homogeneous population than clusters with $\Delta m_{12} \lesssim 1$. The stronger cool cores, more concentrated mass distribution, and non-boxy BCGs, all point towards high- Δm_{12} clusters forming at early times. Such early formation is required to allow sufficient time to pass for the BCG to ingest (aided by dynamical friction) the bright cluster galaxy population in order to develop the large luminosity gap, and for the establishment of the cool core. The formation of more concentrated dark matter halos at earlier times than less-concentrated halos is a generic prediction of cold dark matter theory (e.g. Neto et al. 2007). The interpretation of disk BCGs is less straightforward, however such morphologies can plausibly be interpreted as evidence for the last major mergers in a BCG's formation history comprising gas-rich galaxies – the presence of gas thus leading to the establishment of a disk-like structure in the BCG. This gas-rich merger scenario for BCG formation is consistent with the early formation of large- Δm_{12} clusters.

How can the heterogeneous population of low- Δm_{12} clusters, and more specifically, the fact that some low- Δm_{12} clusters have strong cool cores, non-boxy BCGs, and high concentrations, be interpreted within the context of the early formation of high- Δm_{12} clusters? The most natural explanation is that large- Δm_{12} clusters can evolve into low- Δm_{12} clusters when the supply of bright cluster galaxies is replenished by episodes of hierarchical infall of smaller galaxy systems, such as galaxy groups. Such infall would depress Δm_{12} and increase f_{sub} immediately that the group entered the measurement aperture (in this case a clustercentric radius of $\sim 0.4r_{200}$), and would modify other cluster properties such as the cool core strength, BCG morphology, and concentration of the mass distribution on longer timescales of several Gyr. The observed heterogeneity of low- Δm_{12} clusters can therefore be explained by these clusters comprising both (i) clusters that have formed more recently, and thus have a low concentration, haven't had time to develop a large luminosity gap and cool core, and have a BCG formed

from relatively gas-poor mergers, and (ii) clusters that formerly had a large luminosity gap, and have suffered hierarchical infall in the previous few Gyr. We therefore conclude that a large luminosity gap (and large substructure fraction) is a phase through which a cluster can evolve if sufficient time elapses between episodes of hierarchical merging of other galaxies and groups of galaxies with the cluster. The large scatter seen in the theoretical age- Δm_{12} and age- f_{sub} relationships (Dariush et al. 2007, 2010; Smith & Taylor 2008) lend further weight to the view that both the age *and* the recent merger history of a cluster contribute to the observed values of Δm_{12} and f_{sub} .

We also compare our observational results with predictions from Millennium simulation-based semi-analytic models of galaxy evolution. We find that none of the models can successfully reproduce the observations in their entirety. Bower et al. (2006) succeeds best at reproducing the monotonically declining $p(\Delta m_{12})$, however they predict a relationship between BCG luminosity and Δm_{12} that is far too steep. In contrast, both Croton et al. (2006) and de Lucia & Blaizot (2007) predict that $p(\Delta m_{12})$ peaks at $\Delta m_{12} \sim 1 - 1.5$, in disagreement with the observations, with de Lucia & Blaizot predicting the more prominent peak. de Lucia & Blaizot also predict $p(\Delta m_{12} \geq 2) \sim 0.17$, in contrast to the observed value of $p(\Delta m_{12} = 0.07^{+0.05}_{-0.03})$. Nevertheless, both Croton et al. and de Lucia & Blaizot match the observed slope of the relationship between BCG luminosity and Δm_{12} very well. We discuss the possible causes of these disagreements, and suggest that Bower et al.'s model may be too efficient at converting cold gas to stars in BCGs, and may also be too efficient at replenishing the supply of galaxies in clusters.

We also note that semi-analytic galaxy evolution models also fail to reproduce observational results on high redshift BCGs (Collins et al. 2009; Stott et al. 2010). Our new results add to this picture of the inability of models to reproduce observations of BCGs. An important strength of our results is that we do not rely on calculations of the stellar mass of BCGs, and thus are insensitive to possible systematic uncertainties in stellar mass estimates for observed BCGs arising from alternative stellar population models.

Our future work on the hierarchical assembly of clusters at $z \simeq 0.2$ will take advantage of the wide-field multi-wavelength dataset that we are assembling, including mid/far-IR observations with *Spitzer* and *Herschel*, joint strong/weak-lens modeling of the cluster mass distributions, our spectroscopic redshift survey of cluster galaxies with MMT/Hectospec, and X-ray observations with *XMM-Newton* and *Chandra*.

ACKNOWLEDGMENTS

We acknowledge helpful comments from the anonymous referee. We thank our LoCuSS collaborators, in particular Alastair Edge, Victoria Hamilton-Morris, Jean-Paul Kneib, Yuying Zhang, and Nobuhiro Okabe, for encouragement, assistance and many stimulating discussions. HGK, GPS, AJRS, TJP, and JPS acknowledge support from PPARC and latterly from STFC. GPS acknowledges support from the Royal Society. GPS thanks Andrew Benson, Richard Bower, Gabriella de Lucia, and Malcolm Bremer for helpful discussions and comments; Kevin Bundy, Brad Cenko, Chris Conselice, Richard Ellis, Avishay Gal-Yam, Sean Moran, David Sand and Keren Sharon for assistance with acquiring some of the near-infrared data presented in this article; and Rick Burruss and Jeff Hickey for their support at Palomar Observatory.

REFERENCES

- Allen S. W., 2003, *Ap&SS*, 285, 247
 Ascasibar Y., Diego J. M., 2008, *MNRAS*, 383, 369
 Bender, R. 1988, *A&A*, 193, 7
 Bender R., Surma P., Doebereiner S., Moellenhoff C., Madejsky R., 1989, *A&A*, 217, 35
 Bertin, E. and Arnouts, S., 1996, *A&A*, 117, 393
 Bildfell, C. and Hoekstra, H. and Babul, A. and Mahdavi, A., 2008, *MNRAS*, 389, 1637
 Böhringer H.; Schuecker, P.; Guzzo, L.; et al., 2004, *A&A*, 425, 367
 Bower R. G. et al. *MNRAS*, 370, 645
 Broadhurst T., Takada M., Umetsu K., et al., 2005, *ApJ*, 619, 143
 Bullock J.S., Kolatt T.S., et al., 2001, *MNRAS*, 321, 559
 Buote D. A., Gastaldello F., Humphrey P. J., Zappacosta L., Bullock J. S., Brighenti, F., Mathews W. G., 2007, *ApJ*, 664, 123
 Cole, S., Norberg, P., Baugh, C. M., Frenk, C. S., Bland-Hawthorn, J., Bridges, T., & Cannon, R. 2001, *MNRAS*, 326, 255
 Collins, C. A. and Stott, J. P. and Hilton, M. and Kay, S. T. and Stanford, S. A. and Davidson, M. and Hosmer, M. and Hoyle, B. and Liddle, A. and Lloyd-Davies, E. and Mann, R. G. and Mehrrens, N. and Miller, C. J. and Nichol, R. C. and Romer, A. K. and Sahlén, M. and Viana, P. T. P. and West, M. J., 2009, *Nature*, 458, 603
 Crawford, C. S. and Allen, S. W. and Ebeling, H. and Edge, A. C. and Fabian, A. C., 1999, *MNRAS*, 306, 857
 Croton D. J. et al., 2006, *MNRAS*, 365, 11
 Cypriano E. S., Mendes de Oliveira C., Sodre Jr. L., 2006, *AJ*, 132, 514
 Dariush A. A., Khosroshahi H. G., Ponman T. J., Pearce F., Raychaudhury S., Hartly W., 2007, *MNRAS*, 382, 433
 Dariush A. A., 2009, PhD Thesis, University of Birmingham, England
 Dariush A. A., Raychaudhury S., Ponman T. J., Khosroshahi H. G., Benson A. J., Bower R. G., Pearce F., 2010, *MNRAS*, in press, arXiv:1002.4414
 de Propriis, R., Stanford, S. A., Eisenhardt, P. R., Dickinson, M., Elston, R., 1999, *AJ*, 118, 719
 Dolag, K., Bartelmann, M., Perrotta, F., Baccigalupi, C., Moscardini, L., Meneghetti, M., & Tormen, G. 2004, *A&A*, 416, 853
 Duffy A. R., Schaye J., Kay S. T., Dalla Vecchia C., 2008, *MNRAS*, 390, 64
 Ebeling H.; Edge, A. C.; Böhringer, H.; Allen, S. W.; Crawford, C. S.; Fabian, A. C.; Voges, W.; Huchra, J. P. 1998, *MNRAS*, 301, 881
 Ebeling, H.; Edge, A. C.; Allen, S. W.; Crawford, C. S.; Fabian, A. C.; Huchra, J. P. 2000, *MNRAS*, 318, 333
 Edge, A. C., Ivison, R. J., Smail, I., Blain, A. W., & Kneib, J.-P., 1999, *MNRAS*, 306, 599
 Edge, A. C., Smith G. P., Sand D. J., Treu T., Ebeling H., Allen S. W., van Dokkum P. G., 2003, *ApJ*, 599, 69
 Egami, E., Misselt, K. A., Rieke, G. H., Wise, M. W., Neugebauer, G., Kneib, J., Le Floch, E., Smith, G. P., Blaylock, M., Dole, H., Frayer, D. T., Huang, J., Krause, O., Papovich, C., Pérez-González, P. G., & Rigby, J. R. 2006, *ApJ*, 647, 922
 Evrard, A. E. and MacFarland, T. J. and Couchman, H. M. P. and Colberg, J. M. and Yoshida, N. and White, S. D. M. and Jenkins, A. and Frenk, C. S. and Pearce, F. R. and Peacock, J. A. and Thomas, P. A., 2002, *ApJ*, 573, 7
 Faber S. M., et al., 1997, *AJ*, 114, 1771

- Gavazzi R., Fort B., et al., 2003, *A&A*, 403, 11
- Gehrels N., 1986, *ApJ*, 303, 336
- Geller, M. J. and Peebles, P. J. E., 1976, *ApJ*, 206, 939
- Gratton, R. G. and Fusi Pecci, F. and Carretta, E. and Clementini, G. and Corsi, C. E. and Lattanzi, M., 1997, *ApJ*, 491, 749
- Hamilton-Morris V. H., et al, 2009, in preparation
- Haines C. P., Smith G. P., et al., 2009, *MNRAS*, 396, 1297
- Haines C. P., Smith G. P., et al., 2009, *ApJ*, 704, 126
- Haines C. P., Smith G. P., et al., 2010, *A&A*, in press, arXiv:1005.3811
- Heckman, T. M., 1981, *ApJ*, 250, 59
- Hernquist L., 1990, *ApJ*, 356, 359
- Jee, M. J.; Ford, H. C.; Illingworth, G. D.; White, R. L.; Broadhurst, T. J.; Coe, D. A.; Meurer, G. R.; van der Wel, A.; Bentez, N.; Blakeslee, J. P., 2007, 2007, *ApJ*, 661, 728
- Jing Y. P., 2000, *ApJ*, 535, 30
- Jing, Y. P.; Suto, Y., 2002, *ApJ*, 574, 538
- Jones L. R., Ponman T. J., Horton A., Babul A., Ebeling H., Burke D. J., 2003, *MNRAS*, 343, 627
- Jones L. R., Ponman T. J., Forbes D.A., 2000, *MNRAS*, 312, 139
- Khochfar S., Burkert A., 2005, *MNRAS*, 359, 1379
- Khosroshahi H. G., Raychaudhury S., Ponman T. J., Miles T. A. Forbes D., 2004, *MNRAS*, 349, 524
- Khosroshahi H. G., Jones L. R., Ponman T. J., 2004, *MNRAS*, 349, 1240
- Khosroshahi H. G., Maughan B., Ponman T. J., Jones L. R., 2006, *MNRAS*, 369, 1211
- Khosroshahi H. G., Ponman T. J., Jones L. R., 2006, *MNRAS Letters*, 372, 68
- Khosroshahi H. G., Ponman T. J., and Jones L. R., 2006, *MNRAS*, 377, 595
- King C. R. and Ellis R. S., 1985, *ApJ*, 288, 456
- Kneib, J-P, et al., 2003, *ApJ*, 598, 804
- Komatsu, E., et al. 2009, *Astronomy*, 2010, 158
- La Barbera, F. and Merluzzi, P. and Busarello, G. and Massarotti, M. and Mercurio, A., 2004, *A&A*, 425, 797
- La Barbera, F. and de Carvalho, R. R. and de la Rosa, I. G. and Gal, R. R. and Swindle, R. and Lopes, P. A. A., 2010, *AJ*, submitted, arXiv:1006.4065
- Limousin, M.; Kneib, J. P.; Bardeau, S.; Natarajan, P.; Czoske, O.; Smail, I.; Ebeling, H.; Smith, G. P., 2007, *A&A*, 461, 881
- Lin Y.-T.; Mohr, J. J.; Stanford, S. A., 2004, *ApJ*, 610, 745
- Lin Y.-T. & Mohr J. J., 2004, *ApJ*, 617, 879
- de Lucia G., Blaizot J., 2007, *MNRAS*, 375, 2
- McCarthy I., Babul A., Bower R. G., Balogh M., 2008, *MNRAS*, 386, 1309
- Mannucci, F.; Basile, F.; Poggianti, et al., 2001, *MNRAS*,
- Mendes de Oliveira C., Cypriano E. S., Sodre Jr. L., 2006, *AJ*, 131, 158
- Miller C. J. et al., 2005, *AJ*, 130, 968
- Milosavljević M., Miller C. J., Furlanetto S. R., Cooray A., 2006, *ApJ*, 637, L9
- Marrone D., Smith G. P., Richard J., et al., 2009, *ApJ*, 701, L114
- Naab T., Burkert A., 2003, *ApJ*, 597, 893
- Navarro J. F., Frenk, C. S., White, S. D. M., 1997, *ApJ*, 490, 493
- Neto A. F., Gao L., Bett P., et al., 2007, *MNRAS*, 381, 1450
- Okabe N., Umetsu K., 2008, *PASJ*, 60, 345
- Okabe N., Takada M., Umetsu K., Futamase T., Smith G.P., 2010, *PASJ*, in press, arXiv:0903.1103
- Okabe N., Zhang Y.-Y., Finoguenov A., Takada M., Umetsu K., Futamase T., 2010, *ApJ*, submitted
- Oegerle, W. R. and Hoessel, J. G., 1989, *AJ*, 98, 1523
- Oguri, M. and Takada, M. and Okabe, N. and Smith, G. P., 2010, *MNRAS*, in press.
- Ostriker, J. P. and Hausman, M. A., 1977, *ApJ*, 217, 125
- Pereira M., Haines C. P., et al., 2010, *A&A*, in press, arXiv:1005.3813
- Ponman T. J., Allan D. J., Jones L. R., Merrifield M., MacHardy I. M., 1994, *Nature*, 369, 462
- Quillen, A. C., Zufelt, N., Park, J., O’Dea, C. P., Baum, S. A., Privon, G., Noel-Storr, J., Edge, A., Russell, H., Fabian, A., Donahue, M., Bregman, J. N., McNamara, B. R., & Sarazin, C. L. 2008, *ApJS*, 176, 39
- Reid, I. N., 1997, *AJ*, 114, 161
- Reiprich T. H. and Böhringer H., 2002, *ApJ*, 567, 716
- Richard J., et al., 2010, *MNRAS*, 402, 44
- Richard J., Smith G. P., et al., 2010, *MNRAS*, 405, 325
- Sandage, A. and Hardy, E., 1973, *ApJ*, 183, 743
- Sanderson, A. J. R., Edge, A. C., & Smith, G. P. 2009, *MNRAS*, 398, 1698
- Sanderson, A. J. R. & Ponman, T. J. 2010, *MNRAS*, 402, 65
- Smith G. P. Kneib J., Smail I., Mazzotta P., Ebeling H., Czoske, O., 2005, *MNRAS*, 359, 417
- Smith G. P., Taylor J. E., 2008, *ApJ*, 682, L73
- Smith G. P., et al., 2009, *ApJ*, 707, 163
- Smith G. P., Haines C. P., et al., 2010, *A&A*, in press, arXiv:1005.3816
- Stott J. P., Edge A. C., Smith G. P., Swinbank A. M., Ebeling H., 2008, *MNRAS*, 384, 1502
- Stott, J. P. and Collins, C. A. and Sahlen, M. and Hilton, M. and Lloyd-Davies, E. and Capozzi, D. and Hosmer, M. and Liddle, A. R. and Mehtens, N. and Miller, C. J. and Romer, A. K. and Stanford, S. A. and Viana, P. T. P. and Davidson, M. and Hoyle, B. and Kay, S. T. and Nichol, R. C., 2010, *ApJ*, in press, arXiv:1005.4681
- Taylor J. E., Babul A., 2004, *MNRAS*, 348, 811
- Vale A., Ostriker J. P., 2007, *astro-ph/0701096*
- Tremaine, S. D. and Richstone, D. O., 1977, *ApJ*, 212, 311
- Vikhlinin, A., Burenin, R., Forman, W. R., Jones, C., Hornstrup, A., Murray, S. S., & Quintana, H. 2007, in *Heating versus Cooling in Galaxies and Clusters of Galaxies*, ed. H. Böhringer, G. W. Pratt, A. Finoguenov, & P. Schuecker, 48–
- Wechsler R. H., Bullock J. S., et al., 2002, *ApJ*, 568, 52
- Wilson J. C., et al., 2003, *SPIE*, 4841, 451
- Zentner, A. R., Berlind, A. A., Bullock, J. S., Kravtsov, A. V., Wechsler, R. H.
- Zhang Y.-Y., Finoguenov A., Böhringer H., Kneib J.-P., Smith G. P., Czoske O., Soucail G., 2007, *A&A*, 467, 437
- Zhang Y.-Y., Finoguenov A., Böhringer H., Kneib J.-P., Smith G. P., Kneissl, R., Okabe, N., Dahle, H., 2008, *A&A*, 482, 451

This paper has been typeset from a $\text{\TeX}/\text{\LaTeX}$ file prepared by the author.